Aversion to nicotine is regulated by the balanced activity of β4 and α5 nicotinic receptor subunits in the medial habenula

Silke Frahm[1], Marta A. Slimak[1], Leiron Ferrarese[1], Julio Santos-Torres[1], Beatriz Antolin-Fontes[1], Sebastian Auer[1], Sergey Filkin[2], Stéphanie Pons[3], Jean-Fred Fontaine[4], Victor Tsetlin[2], Uwe Maskos[3], Inés Ibañez-Tallon[1]*

[1]*Department of Molecular Neurobiology, Max-Delbrück-Centrum, Robert-Rössle-Str. 10, 13125 Berlin, Germany.*

[2]*Shemyakin-Ovchinnikov Institute of Bioorganic Chemistry, Russian Academy of Sciences, Moscow, Russia.*

[3]*CNRS URA 2182, Département de Neurosciences, Institut Pasteur, 25 rue du Dr Roux, 75724 Paris Cédex 15, France.* [4]*Computational Biology and Data Mining Group, Max-Delbrück-Centrum, Robert-Rössle-Str. 10, 13125 Berlin, Germany.*

*Correspondence: ***ibanezi@mdc-berlin.de***

Running title: Determinants of α3β4α5 nAChRs in nicotine aversion

SUMMARY

Nicotine dependence is linked to single nucleotide polymorphisms in the *CHRNB4-CHRNA3-CHRNA5* gene cluster encoding the α3β4α5 nicotinic acetylcholine receptor (nAChR). Here we show that the β4 subunit is rate-limiting for receptor activity, and that current increase by β4 is maximally competed by one of the most frequent variants associated with tobacco usage (D398N in α5). We identify a β4 specific residue (S435), mapping to the intracellular vestibule of the α3β4α5 receptor in close proximity to α5 D398N, that is essential for its ability to increase currents. Transgenic mice with targeted overexpression of *Chrnb4* to endogenous sites display a strong aversion to nicotine that can be reversed by viral-mediated expression of the α5 D398N variant in the medial habenula (MHb). Thus, this study both provides novel insights into α3β4α5 receptor mediated mechanisms contributing to nicotine consumption, and identifies the MHb as a critical element in the circuitry controlling nicotine dependent phenotypes.

INTRODUCTION

Tobacco use is a major public health challenge leading to millions of preventable deaths every year (http://www.nida.nih.gov/researchreports/nicotine/nicotine.htm). The principal addictive component of tobacco is the plant alkaloid nicotine that binds and activates nicotinic acetylcholine receptors (nAChRs) (Dani and Heinemann, 1996). In the mammalian nervous system, eight alpha (α2-α7, and α9-α10) and three beta (β2-β4) subunits assemble into pentameric nAChR combinations with distinctive pharmacological and functional properties (Gotti et al., 2009; McGehee and Role, 1995). Recently, genome-wide association studies (GWAS) have identified genetic variants in the *CHRNB4/A3/A5* gene cluster as risk factors for nicotine dependence and lung cancer (Amos et al., 2010a; Saccone et al., 2009; Thorgeirsson et al., 2008; Weiss et al., 2008). These single nucleotide polymorphisms (SNPs) include non-coding variants across the gene cluster, as well as amino acid substitutions (http://www.ncbi.nlm.nih.gov/snp/). Given that *cis*-regulatory elements within the cluster coordinate transcription of these genes for assembly of α3β4-containing (α3β4*) and α3β4α5 functional nAChRs (Scofield et al., 2010; Xu et al., 2006), the fact that a large number of SNPs map to non-coding segments of the cluster suggests that altered regulation of these genes can contribute to the pathophysiology of tobacco use. Indeed the risk for nicotine dependence seems to stem from at least two separate mechanisms: the variability in the mRNA levels of these genes and functional changes due to non-synonymous amino acid variants (Lu et al., 2009).

A number of mouse models with gene deletions, point mutations or strain-specific variants in nAChR subunits have been critical to elucidate the role of the different nAChR combinations in nicotine addiction and withdrawal. For instance, α4β2 nAChRs, accounting for 80% of the high affinity nicotine-binding sites in the brain (Whiting and Lindstrom, 1988), are major contributors to nicotine self-administration, as shown in β2 knockout (KO) mice (Maskos et al., 2005; Picciotto, 1998) and in knock-in mice with a gain-of-function mutation of α4 (Tapper et al., 2004). The nAChR β4 subunit is almost always co-expressed with α3, while the auxiliary α5 subunit assembles with the α3β4 combination, but can also be incorporated in α4β2 receptor

complexes. The expression of the α3β4* nAChR combination is restricted to a few discrete brain areas including the medial habenula (MHb) and interpeduncular nucleus (IPN), and to autonomic ganglia (Zoli et al., 1995). α3β4* nAChRs have a lower affinity for nicotine than α4β2 receptors and are likely less desensitized at the nicotine levels found in smokers than α4β2 nAChRs, suggesting that α3β4* nAChR could play an important role in tobacco addiction, since they retain their sensitivity to fluctuating nicotine levels in smokers (Rose, 2007). β4 and α5 KO mice show similar phenotypes including decreased signs of nicotine withdrawal symptoms (Jackson et al., 2008; Salas et al., 2004; Salas et al., 2009), hypolocomotion and resistance to nicotine-induced seizures (Kedmi et al., 2004; Salas et al., 2004). It has been more difficult to assess the role of α3* nAChRs since KO mice die within 3 weeks after birth due to severe bladder dysfunction (Xu et al., 1999).

Here we show that α3β4α5 nicotinic acetylcholine receptor activity in *vitro* and *in vivo* is limited by the level of *Chrnb4* expression, and that the ability of the β4 subunit to increase α3β4α5 currents depends on a single, unique residue (S435). This residue maps to the intracellular vestibule of the nAChR complex adjacent to the rs16969968 SNP in *CHRNA5* (D398N), linked to a high risk of developing nicotine dependence in humans. We present a novel transgenic mouse model of the *Chrnb4-Chrna3-Chrna5* gene cluster, referred to as Tabac (Transgenic a3b4a5 cluster) mice, in which *Chrnb4* overexpression enhances α3β4* nAChR levels, resulting in altered nicotine consumption and nicotine-conditioned place aversion. Lentiviral-mediated transduction of the medial habenula of Tabac mice with the D398N *Chrna5* variant reversed the nicotine aversion induced by β4 overexpression. This study provides a new mouse model for nicotine dependence, demonstrates a critical role for the MHb in the circuitry controlling nicotine consumption, and elucidates novel molecular mechanisms contributing to these phenotypes.

RESULTS

The relative levels of α5 and β4 subunits strongly affect α3β4α5 nAChR currents

Recently it has been shown that α5 competes with β4 for association with α4, and that this competition does not occur if β4 is substituted by β2 (Gahring and Rogers, 2010). Given that the *CHRNA5-A3-B4* gene cluster regulates the co-expression of α5, β4 and α3 subunits, and that SNPs in the cluster regulatory regions as well as non-synonymous variants such as rs16969968 (corresponding to D398N in *CHRNA5),* associate with nicotine dependence (Bierut, 2010; Bierut et al., 2008; Saccone et al., 2009), we were first interested in determining whether variation of the proportion of α3, β4 and α5 (Wildtype and D398N) subunits influences nicotine evoked currents. To measure this, we performed electrophysiological recordings in oocytes injected with cRNA transcripts of the different mouse subunits. In these experiments (Figure 1), the cRNA concentration of α3 was held constant (1 ng/ oocyte), whereas the concentration of β4 or β2 input cRNA was varied from 1, 2, 4, 5 to 10 ng, respectively. These experiments showed that β4, but not β2 was able to increase current amplitudes in a dose dependent manner (Figures 1A and 1B). β4 overexpression did not shift the dose response curves for nicotine (Figure S1A). Next we held constant the concentrations of α3 and β4 at 1:10 and added the cRNA of α5 Wildtype (Wt) or of the α5 D397N variant (corresponding to the human α5 variant D398N) at ratios of 1:10:1, 1:10:5 and 1:10:10 (Figure 1A). We observed a significant decrease of current amplitudes at higher concentrations of α5 and this effect was significantly more pronounced with α5 D397N. These results suggest that α5 and β4 may compete for binding to α3, in line with the studies showing such competition for binding to α4 (Gahring and Rogers, 2010).

Given that overexpression of β2 with either α3 (Figure 1A) or α4 (Figure S1B) did not increase currents, we were interested in identifying the residues differing between β4 and β2 that

mediate this effect. Since the long cytoplasmic loop is the most divergent domain between nAChR subunits (Figure S1C), and since it has been implicated in cell-surface expression and trafficking of β2 subunits (Nashmi et al., 2003; Ren et al., 2005), we generated β2-β4 chimeras exchanging either this domain, or short motifs and single residues within this domain. Replacement of the cytoplasmic loop of β2 with the corresponding sequences present in β4 (β2/β4 322-496) led to strong increase of nicotinic currents (Figure 1C). Introduction of two β4 specific motifs (a serine/tyrosine rich motif (β2/+β4 382-391) and gephyrin-like-binding motif (β2/+β4 401-419) into the β2 loop had no influence on current amplitudes (Figure 1C). We next performed bioinformatic analyses and singled out eight β4 specific residues (indicated as T-1 to T-8 in Figure S1C) present within highly conserved motifs. Six of these residues were not further considered: T-2, T-3, T-6 and T-7 residues differ between mouse and chicken β4 subunits which are equally potent in enhancing nicotine-evoked currents (Figure S1B); T-4 residue lies within the tested motif in the β2/+β4 382-391 chimera; and residues at position T-8 have the same charge (Figure S1C). The remaining 2 candidates T-1 (S324 in β4 and T327 in β2) and T-7 (S435 in β4 and R431 in β2) (Figure S1C) were tested by point mutagenesis in the β2 subunit backbone. The β2 T327S point mutant did not increase current, whereas replacement of β2 R431 with serine resulted in a 3,5 fold current increase (Figure 1C). Furthermore, point mutation of the native S435 in the β4 subunit to the arginine residue present in β2 (β4 S435R) abolished the β4 specific activity. Thus, these data demonstrate that the distinctive ability of β4 to increase currents when overexpressed maps to a single residue (S435) that is both required in β4 for current increase, and that can confer this property to β2.

Electrostatic mapping of the intracellular vestibule of the α3β4α5 nAChR complex

Alignment of mouse, human and *Torpedo* nAChR subunit sequences indicated that S435 in β4 and D397N in α5 are located in the 25 aminoacid long amphipathic membrane-associated stretch (MA-stretch) described in the Torpedo subunits (Unwin, 2005) (Figure 2A). Electron microscopy

studies of the Torpedo nAChR have proposed a three-dimensional density map of the receptor complex. In particular, these analyses predict that the MA-stretch of each subunit forms a curved α-helix that collectively create an inverted pentagonal cone vestibule. To locate the S435 (β4) and D397 (α5) residues within the receptor pentamer, we performed homology modeling with the *Torpedo* nAChR using one possible α3β4α5 subunit arrangement. This model predicted the formation of a very similar disposition of α-helices in the α3β4α5 and mapped both residues to the intracellular vestibule (Figure 2B). Electrostatic mapping of the vestibule showed a particular disposition of charges with S435 and D397 located at the more distal and positively charged part of the vestibule (Figure 2C). These data indicate: first that the critical residue in β4 that mediates the β4 effect is located in the receptor structure near the α5 most common SNP associated to heavy smoking; second that this is a highly charged domain of the receptor where single residue changes may have a particularly strong effect on receptor activity.

Transgenic mice of the *Chrnb4/a3/a5* gene cluster (Tabac mice)

To test the hypothesis that β4 is rate-limiting for nAChR assembly and function *in vivo* and that overexpression of β4 can strongly influence nicotine-evoked currents and behavioral responses to nicotine, we characterized a BAC transgenic line spanning the *Chrnb4-Chrna3-Chrna5* gene cluster (Gong et al., 2003). The BAC transgene included the intact coding sequences of the *Chrnb4* gene, modified sequences of *Chrna3* and incomplete sequences of *Chrna5. Chrna3* was modified by insertion of an eGFP cassette followed by polyadenylation signals at the ATG translation initiator codon of *Chrna3* (Figure 3A). The upstream sequences of *Chrna5*, encoding exon 1 splice variants (Flora et al., 2000), are missing in the BAC transgene (Figure 3A). To promote correct expression of *Chrnb4*, the BAC included the intergenic and 5' flanking regions encompassing the *cis*-regulatory elements that coordinate co-transcriptional control of the genes in the cluster (Bigger et al., 1997; Medel and Gardner, 2007; Xu et al., 2006). As a result of these modifications in the BAC transgene, these mice (referred to as Tabac mice for Transgenic a3b4a5 cluster) express high levels of β4 but not α5 (Figure 3B), and expression of α3 is

replaced by expression of an eGFP reporter cassette to monitor the sites expressing the transgene (Figures 3C-H). As shown in figure 3, neurons expressing eGFP were evident in autonomic ganglia (Figure 3C), and in very restricted brain structures (Figures 3D-H) known to express these genes (Zoli et al., 1995). Immunostaining with cholinergic (ChAT) and dopaminergic (TH) markers indicated high expression of *Chrna3*/eGFP in cholinergic neurons of the Hb-IPN system (Figures 3G and 3H). Intense *Chrna3*/eGFP expression was also detected in other brain areas (Figures 3D and 3E) involved in nicotine addiction such as the VTA, the caudal linear nucleus (Cli), the supramammilary nucleus (SuM)(Ikemoto et al., 2006) and the laterodorsal tegmental nucleus (Figure 3F), which provides modulatory input to the VTA (Maskos, 2008). We performed *in situ* hybridization experiments to verify that the BAC accurately directed expression of transgenic *Chrnb4* transcripts to eGFP positive brain areas. Tabac mice showed a prominent enrichment of *Chrnb4* transcripts in $\alpha 3\beta 4$* positive areas such as MHb and IPN and in brain areas that have been shown to express lower levels of *Chrnb4* such as SuM (Dineley-Miller and Patrick, 1992) and VTA (Yang et al., 2009) (Figures 3I and 3J). RT-PCR studies showed that *Chrna4*, *Chrna7*, and *Chrnb2* transcripts (which are not present in the BAC) are not altered in Tabac mice (Figure S2). Taken together these data show that Tabac mice express high levels of $\beta 4$, but not $\alpha 5$, in $\alpha 3$/eGFP labeled cells in CNS and PNS structures known to express the *Chrnb4-Chrna3-Chrna5* nicotinic gene cluster, thus providing a useful mouse model to test the consequences of enhanced $\beta 4$ expression at endogenous sites.

Increased nicotine-evoked currents in transgenic Tabac mice

Given the demonstration that the level of $\beta 4$ expression is rate-limiting for the function of $\alpha 3\beta 4\alpha 5$ receptors *in vitro* (Figure 1), we were next interested in determining whether enhanced expression of *Chrnb4* in Tabac neurons resulted in elevated nicotine-evoked currents *in vivo*. Previous studies have shown that neurons in the MHb express high levels of $\alpha 3\beta 4\alpha 5$ receptors (Quick et al., 1999). Accordingly, we employed patch clamp recordings to measure nicotine-evoked currents in MHb neurons of Tabac mice. A large proportion of MHb neurons in Wt mice (*n*

= 20 of *n* = 23 neurons recorded) responded to local fast application (50 ms) of nicotine (Figures 4A and 4B). In *Chrna3*/eGFP labeled MHb neurons of Tabac mice, nicotine elicited significantly increased peak currents in comparison to Wt littermates (on average, 3.4 fold at 100 μM nicotine, two-way ANOVA $P < 0.05$) (Figure 4B). Similarly increased responses were obtained using acetylcholine (ACh) (data not shown). Dose-response curves for nicotine showed no significant differences between Wt and Tabac mice, indicating that the affinity of the receptors in the transgenic mice is not altered (Figure 4C). Application of mecamylamine (MEC), a non-selective potent inhibitor of α4β2* and α3β4* nAChRs (Bacher et al., 2009), resulted in a blockade of as much as 90% of the nicotine-elicited responses in Tabac mice (Figure 4D), demonstrating that the enhanced nicotine responses in Tabac neurons result directly from elevated levels of functional nAChRs. To determine whether these additional receptors cause enhanced neuronal excitability, the firing rate of habenular neurons was measured in current clamp assays in response to nicotine. Neurons from Wt and Tabac mice were silent at rest (-70 mV). Local nicotine application (1 μM for 3 sec) elicited single action potentials in Wt neurons, whereas nicotine induced a robust burst of action potentials with a 13-fold higher firing frequency on average in Tabac neurons ($P < 0{,}005$) (Figures 4E and 4F). Together, these results indicate that the increased sensitivity of MHb neurons to nicotine in Tabac mice results from the presence of additional functional nAChRs, rather than from changes in the nicotine affinity of existing receptors.

Tabac mice have increased α3β4* nAChR binding sites

To assay for elevated receptor expression across different brain structures, we performed autoradiographic radioligand binding assays with iodinated epibatidine, which mainly binds α4β2* and α3β4* nAChRs (Perry and Kellar, 1995) (Figures 5A and 5B). Competition with cold cytisine, which binds with higher affinity to α4β2* than to α3β4* receptors (Marks et al., 2010), was done to distinguish α3β4* from overlapping α4β2* binding sites (Zoli et al., 1998) (Figures 5C and 5D). In

Wt mice, discrete brain regions resistant to cytisine competition labeled well-known $\alpha3\beta4$* sites such as MHb, IPN and superior colliculus (Figure 5C). In Tabac mice, increased radioligand binding to cytisine-resistant sites was detected in these areas, and in additional brain structures including the VTA, SuM, substantia nigra and striatum (Figure 5D). A strong correlation between radioligand signal and eGFP fluorescence was detected in all analyzed CNS structures (Figure 5E and Table S1). Densitometric analyses indicated significantly increased cytisine-resistant signals in $\alpha3\beta4$* expressing regions in Tabac mice (Table S1) while $\alpha4\beta2$* epibatidine-binding sites such as cortex and thalamus did not differ between control and Tabac mice (Figures 5A and 5B), indicating that elevated surface receptors are present in sites corresponding to endogenous $\beta4$ expression sites. To exclude the possibility that the increased radioligand signal could reflect increased cell number, we quantified the cell density in MHb of Tabac and Wt mice and observed no significant differences (Figure S3). These data show that the enhanced nicotine-evoked currents in Tabac mice result from $\beta4$ mediated recruitment of additional functional $\alpha3\beta4$* nAChR complexes on the cell surface.

Taken together, the anatomic mapping and in situ hybridization results presented in Figure 3 and the receptor binding assays presented in Figure 5 provide compelling evidence that $\alpha3\beta4$* nAChRs are located both on the cell soma and in the axon termini. For example, the relatively light staining of the IPN by ISH in Tabac mice strongly suggests that the very heavy expression of functional $\alpha3\beta4$* receptors, detected in this structure by receptor binding results from both local synthesis in the IPN and the presence of receptors synthesized in the MHb and transported to presynaptic termini in the IPN. This is consistent with the well documented effects of presynaptic nAChRs on synaptic release and neurotransmission (McGehee et al. 1995), and suggests that Tabac mice will be an important tool for further dissection of the roles of pre- and postsynaptically expressed nAChRs.

Tabac mice show strong aversion to nicotine consumption, and display nicotine conditioned place aversion

We were next interested in the effects of elevated nAChR expression on the behavioral

responses of Tabac mice to nicotine. Measurements of drinking volumes showed that Tabac mice consumed significantly less nicotine containing water than Wt littermates (Figures 6A and 6B). Because nicotine solutions have a bitter taste, nicotine was diluted in saccharin solution and control experiments with a bitter solution (containing quinine) were performed. There were no differences in consumption of regular, sweetened or bitter water between the two groups (Figure 6A). Next, we performed a free choice consumption experiment where mice were allowed to choose between regular water and water supplemented with different concentrations of nicotine (1-100 μg/ml) without saccharin. Analysis of the nicotine volume consumed relative to the total fluid intake (Figure 6C) indicated that Tabac mice significantly avoided drinking nicotine solutions containing more than 5 μg/ml nicotine ($P < 0.05$, two-way ANOVA), while Wt showed no preference between water and nicotine solutions below 50 μg/ml and avoided drinking the highest concentration of nicotine solution tested. It is possible that the decrease in drinking is due to negative consequences of hyperactivation of the autonomic nervous system leading to gastric distress or nausea. However, we observed no significant differences in body weight (Figure 6D) micturition and digestion (Figure S4) before and during the nicotine consumption experiments.

As an independent measure of the effects of nicotine in Tabac mice, conditioned place aversion (CPA) assays were performed. Because conditioning to nicotine is both concentration and strain dependent (O'Dell and Khroyan, 2009) we measured CPA in Wt C57BL/6 littermates at 0.5 mg nicotine/ kg body weight. Under these conditions, we observed neither a preference nor aversion to nicotine. In contrast, strong conditioned place aversion to nicotine was observed in Tabac mice (Figure 6E). These data both confirms the conclusions of the nicotine consumption assays, and demonstrates that negative reward learning associated to nicotine is strongly increased in Tabac mice. We conclude that overexpression of the β4 subunit *in vivo* leads to an increase in functional α3β4* receptors, resulting in a higher sensitivity to the aversive properties of nicotine.

Lentiviral-mediated expression of the α5 D397N variant in the medial habenula reverses nicotine aversion in Tabac mice

The observations that the α5 D397N variant reduces α3β4α5 nicotine-evoked currents in oocytes (Figure 1), and that the MHb contains a high density of native α5 nAChR subunits in combination with α3β4 subunits (Figure 3), suggested that the enhanced nicotine aversion evident in Tabac mice could be reversed by expression of the α5 variant in the MHb. To test this hypothesis we employed lentiviral-mediated transduction to express the α5 D397N in MHb neurons of Tabac mice. We injected bilaterally either control lentivirus (LV-PC) or the LV-α5 D397N (LV- α5N) viruses in Tabac mice. As shown in Figure 7B, immunostaining for the mCherry reporter of LV-α5N expression or direct fluorescence derived from the control lentivirus demonstrated that the lentiviral transduced area corresponds with that occupied by α3β4*-eGFP labeled neurons in the MHb of Tabac mice. Given that the maximal difference in nicotine consumption in Tabac mice occurred at 25 μg/ml nicotine (Figure 6C), mice were again given a two-bottle choice test to measure nicotine aversion. These experiments were performed in Tabac mice backcrossed to the inbred mouse line C57/BL6 (Figure 7C), which has been shown to have a high basal level of self-selection of nicotine (Glatt et al., 2009; Meliska et al., 1995; Robinson et al., 1996), and in Tabac mice outbred between FBV/N mixed and Swiss Webster (Figure 7D). As shown in Figure 7C, in C57/BL6 Tabac mice injection of the LV-α5N virus reversed their nicotine aversion in comparison to mice injected with the control virus. In outbred Tabac mice we observed no alteration in nicotine aversion in Tabac mice injected with the control virus (Figure 7D) with respect to uninjected Tabac mice (Figure 6C). Importantly, infection with LV-α5N virus reversed nicotine aversion in Tabac mice (Figure 7D), restoring nicotine consumption in α5D397N infected Tabac mice to levels evident in Wt mice (Figure 6C). These results demonstrate a major role for the MHb in nicotine consumption.

DISCUSSION

Human genetic studies have established an association between the *CHRNB4-CHRNA3-CHRNA5* locus and tobacco use (Amos et al., 2010b; Saccone et al., 2009; Thorgeirsson et al., 2008; Weiss et al., 2008). Here we report a novel mouse model (Tabac mice) with altered nicotine consumption and conditioned place aversion caused by elevated levels of β4, enhanced nicotine-evoked currents and increased surface expression of functional nAChRs at endogenous sites. The ability of β4 to enhance nicotine-evoked currents depends on a single critical residue (S435) located in the intracellular vestibule of the receptor. Interestingly, modeling studies revealed that one of the most common SNPs associated with tobacco usage, D398N in the α5 subunit, also maps to this domain. Functional analyses of this variant demonstrate that alterations in this domain can result in profound effects on nicotine-evoked currents. Based on our studies in Tabac mice in which enhanced current is associated with increased aversion to nicotine, we predicted that the α5 variant (corresponding to D397N in mice) should increase nicotine consumption consistent with its association with smoking. To test this idea, and given that the MHb contains a very high concentration of endogenous α3β4α5 receptors as well as elevated levels of β4 driven by the Tabac transgene, we introduced the α5 variant by viral-mediated transduction in habenular neurons of Tabac mice. The reversal of the nicotine aversion achieved in Tabac mice observed in these experiments demonstrates that the MHb plays a major regulatory role in nicotine consumption.

Three main points are addressed in this study. First, changes both in the coordinated expression of α3β4α5 subunits (i.e. overexpression of the β4 subunit) as well as in single residues (i.e. *in vivo* viral-mediated expression of the α5 D397N variant) have a strong influence on nicotine consumption in mice. This is consistent with recent genome wide association studies which have identified SNPs in both regulatory and coding regions of the *CHRNB4-CHRNA3-CHRNA5* gene cluster that are associated with nicotine dependence (Levitin et al., 2008; Saccone et al., 2009; Thorgeirsson et al., 2008). Thus our studies provide a new model for further exploration of the involvement of α3β4α5 nAChR function in nicotine consumption.

Second, our studies demonstrate that the intracellular vestibule of the α3β4α5 receptor exerts an important effect on nicotine-evoked currents. The high concentration of charges in this

membrane-associated domain is conserved in the superfamily of Cys-loop receptors (Carland et al., 2009; Kelley et al., 2003; Unwin, 2005). Electrostatic calculations by homology with the *Torpedo* nAChR predict that $\alpha3\beta4\alpha5$ receptors form a highly electronegative vestibule most likely to promote a stabilizing environment for cation outflow. The change in current amplitude produced by substitutions of charged residues (S435R and D397N) in this domain of the receptor predicts that alterations of the electrostatic charge of the vestibule are critical for receptor function. This is consistent with studies of the inner vestibule in other Cys-loop receptor channels. For example, in 5HT3A receptors substitution of arginine positive residues increased channel conductance, whereas introduction of basic residues in this domain of $\alpha1$ glycine receptors decreases glycine evoked currents (Carland et al., 2009; Kelley et al., 2003). Numerous reports have linked the $\alpha5$ D398N polymorphism to smoking incidence (Bierut, 2010; Bierut et al., 2008; Saccone et al., 2009). Incorporation of D398N $\alpha5$ variant into $\alpha4\beta2$ containing receptors in transfected cells results in a two-fold reduction in epibatidine evoked calcium currents without a change in surface expression (Bierut et al., 2008), consistent with the reduction in nicotine-evoked current amplitudes reported here upon incorporation of this variant into $\alpha3\beta4$ containing nAChRs. Taken together, these observations support the hypothesis that substitution of this charged residue modifies the vestibule electrostatic charge but not the number of receptors incorporated into the plasma membrane. In contrast, the increase in receptor surface expression in Tabac mice and the identification of a single residue in the $\beta4$ subunit (S435R) that is both essential for the increase of currents observed in this study upon overexpression of the $\beta4$ subunit, and that can confer this property upon $\beta2$ subunits, suggest that the $\beta4$ subunit is rate-limiting for the formation of $\alpha3\beta4\alpha5$ nAChRs. Although the precise role of S435 is not yet clear, it may be involved in stabilization of nAChR complexes, export of the receptors from the ER due to interactions with trafficking proteins, or alterations in its turnover from the cell surface. For example, rapsyn binding to the α-helical domains corresponding to the inner vestibule of $\alpha1\beta1\gamma\delta$ nAChR is required for surface expression of this receptor (Lee et al., 2009), and binding of UBXD4 to the cytoplasmic loop of $\alpha3$ can interfere with its ubiquitination and, consequently, the

number of α3 containing receptors at the cell surface (Rezvani et al., 2010). Thus, our studies point to two mechanisms mediated by specific residues in the inner vestibule, one leading to ion permeation changes within a single α3β4α5 receptor and the other leading to increased surface expression of receptors by native β4.

Third, the studies presented here demonstrate that the MHb has a major influence in the control of nicotine consumption, extending previous studies of the role of the habenula in nicotine withdrawal and drug addiction (Jackson et al., 2008; Salas et al., 2004; Salas et al., 2009; Taraschenko et al., 2007) and, recently, in nicotine self-administration (Fowler et al., 2011). Although multiple interconnected brain regions, including the prefrontal cortex, VTA, thalamus, striatum and amygdala are affected by chronic use of nicotine, the habenular system is emerging as an important station in pathways regulating the behavioral effects of nicotine (Changeux, 2010; De Biasi and Salas, 2008; Rose, 2007). The MHb projects mainly to the IPN, which, in turn, seems to inhibit the motivational response to nicotine intake. Thus, inactivation of the MHb and IPN both result in increased intake of nicotine (Fowler et al., 2011). Consistent with these studies, overexpression of β4 results in enhanced activity of the MHb resulting in the opposing effect, e.g. aversion to nicotine. Reversal of nicotine aversion in Tabac mice overexpressing β4 is achieved by expression of the α5 D397N in MHb neurons. Similarly, α5 re-expression in the habenula of α5 KO mice normalizes their nicotine intake (Fowler et al., 2011). Taken together, these studies provide direct evidence that the MHb acts as a gate-keeper in the control of nicotine consumption and that the balanced contribution of β4 and α5 subunits is critical for this function. Further analyses of nAChR function in the habenulo-IPN tract and its associated circuitry will be required to fully understand the addictive properties of nicotine.

EXPERIMENTAL PROCEDURES

Two-electrode voltage clamp recordings of *Xenopus* oocytes. cDNA clones of the nAChR mouse subunits α3, α4, α5, β2 and β4 were subcloned into *pCS2*+ plasmid for X*enopus* oocyte

expression and in vitro transcribed with T7 or SP6 RNA polymerases (mMESSAGE mMACHINE, Ambion, Austin, TX) as described in Ibanez-Tallon et al., 2004. β4 S435R, α5 D397N and β2/β4-chimeras were cloned using a Mutagenesis Kit according to the manufacturer instructions (Stratagene). Oocytes were surgically removed and prepared as described (Stürzebecher et al. 2010). Each oocyte was injected with 20 nl of a cRNA mix containing either 1ng or 10ng of one α and one β nAChR-subunit in 1:1, 1:2, 1:3, 1:4, 1:5, 1:10 and 10:1 ratios. In a separate experiment, α5 Wt and α5 D397N were co-injected at 1:10:1, 1:10:5 or 1:10:10 ratios (α3: β4:α5). Macroscopic currents were recorded between 2 and 5 days after injection with a GeneClamp 500B amplifier (Axon Instruments) using a two-electrode voltage clamp with active ground configuration. Electrodes (0.5-2 MΩ) were filled with 3M KCl. The extracellular recording solution contained: 82,5mM NaCl, 2mM KCl, 1mM $CaCl_2$, 1mM $MgCl_2$ and 10mM HEPES at pH 7.4. Nicotine-tartrate (Sigma-Aldrich) was prepared in extracellular solution at concentrations of 10 nM to 100 mM. Solutions were gravity fed with a flow rate of ~5 ml/min using a Bath Perfusion System valve controller (ALA-VM8, Ala Scientific Instruments). Data was acquired using pCLAMP9 software (Axon instruments) and currents were sampled at 10Hz. Membrane potential was clamped to -70mV; only oocytes with leak currents $<$100 nA were used. Mean fold current increase was evaluated by dividing peak amplitudes of 5 – 10 single oocytes at each ratio by peak amplitudes at 1:1 ratio. All experiments were repeated twice. Dose-response curves were calculated relative to the maximal response to nicotine as described in Ibanez-Tallon et al., 2002.

Molecular modeling. All models of pentameric α3α5β4 nAChR and single residue variations were constructed with the program MODELLER 9v7, using the structure of the nAChR from *T.marmorata* (PDB ID 2BG9) as a template for modeling. Energy equilibration and dynamics calculations were performed using GROMACS 3.3.3 applied to a pentameric α3α5β4 nAChR without the extracellular domain. After relaxation an energy equilibration in OPLS-AA force field, the nAChR structures were compared.

Animals. Transgenic Tabac reporter mice were generated as described (Gong et al., 2003). Briefly, a bacterial artificial chromosome RP23-33606, containing the mouse *Chrnb4*, *Chrna3* and *Chrna5* nicotinic receptor gene cluster was recombined using BAC engineering system, by introducing an eGFP and a polyadenylation signal directly upstream of the coding sequence of the *Chrna3* gene. The modified BAC was injected into pronuclei of FVB/N fertilized oocytes and hemizygous progeny was mated to Swiss Webster mice each generation thereafter. For stereotactic injection experiments and CPA, mice were backcrossed to C57BL/6 for 6 generations. All transgenic animals used for experiments were heterozygous. Mice were housed with *ad libitum* access to food and water in room air conditioned at 22-23°C with a standard 12h light/dark cycle, maximal five animals per cage. All procedures were in accordance with ethical guidelines laid down by the local governing body.

Western blotting. Western blotting procedure was adapted from Grady et al. 2009. Briefly, the MHb was dissected from adult Tabac and Wt mice (*n* = 3 per genotype), collected in 1 ml of lysis buffer (50 mM Na phosphate pH 7,4, 1 M NaCl, 2 mM EDTA, 2 mM EGTA and protease inhibitor cocktail) and immediately homogenized by passing the tissue 10 times through a syringe (27 gauge). The homogenates were centrifuged for 30 min at 13,000 rpm and the pellet was resuspended in 500 µl of 50 mM Tris HCl pH 7, 120 mM NaCl, 5 mM KCl, 1 mM MgCl2, 2.5 mM CaCl2 containing protease inhibitor cocktail. After addition of 2 % Triton X-100, the membranes were extracted for 2h at 4°C. Supernatants were recovered after 10 min centrifugation. Equal amounts of membrane extracts underwent SDS-PAGE and were transferred to PVDF membranes. Primary antibodies used were rabbit anti-beta4 (gift from Dr. Cecilia Gotti), mouse monoclonal (268) alpha5 mAb (Abcam, Cambridge, UK) or mouse monoclonal anti-α-Tubulin (Sigma, St Louis, MO, USA). After incubation with the appropriate HRP-conjugated secondary antibodies, peroxidase was detected using a chemiluminescent substrate (Pierce, Rockford, IL, USA).

Brain immunohistochemistry. Adult mice were injected with a lethal dose of ketamine and perfused transcardially with 4% paraformaldehyde in cold 0.1 M phosphate buffer (PB). Brains were fixed for 2-4 hrs and transferred to 30% sucrose in PB. Next day, 40 μm coronal or saggital sections were cut from a dry ice-cooled block on a sliding microtome (Leica) and kept in cryoprotectant (25% ethylene glycol, 25% glycerol and 0.05 M PB) at -20°C until immunofluorescence labeling was performed. Selected brain sections were washed in PBS and pretreated with blocking buffer (0.3% TritonX-100 and 10% horse serum in PBS). All antibodies were diluted in PBT containing 0.3% TritonX-100 and 1% horse serum in PBS. Primary antibodies used were rabbit polyclonal anti-EGFP (Molecular Probes) and goat polyclonal anti-CHAT (Chemicon), both diluted 1:1000, rabbit polyclonal anti-calbindin D-28K (Swint) diluted 1:500, rabbit polyclonal anti-Substance P (Zymed) diluted 1:1000 or mouse monoclonal anti-Tyrosine hydroxylase (Sigma-Aldrich) diluted 1:2000 and incubated overnight at 4 °C. Co-staining with anti-eGFP was necessary to detect fluorescent signals in weak *Chrna3* expression areas (eg. Substantia nigra and VTA) and to visualize axonal/dendritic processes. Secondary antibodies used were, respectively, goat anti-mouse IgG conjugated with Cy3 (Jackson) and donkey anti-goat IgG conjugated with Alexa555 (Molecular Probes), both diluted 1:500 and incubated 2 hrs at RT. Sections were washed, mounted on slides and coverslipped in immu-mount (Thermo Scientific). Fluorescent signals were detected using a confocal laser scanning microscope (Leica SP5). A Biorevo fluorescent microscope (Keyence) was used for low magnification pictures.

***In situ* hybridization.** A mouse brain cDNA library was used to amplify bases 982-1382 from Chrnb4 and subcloned into the TOPO TA pCR2.1 vector (Invitrogen). After linearization, antisense riboprobes were synthesized using T7 RNA polymerase and labeled with DIG according to the manufacturer instructions (Roche Applied Science). *In situ* hybridization was performed on 20 μm coronal sections from Wt and transgenic littermates as described before (Auer et al. 2010). The developing enzymatic color-reaction was stopped simultaneously in sections of Wt and transgenic mice.

Acute brain slice electrophysiological recordings. Whole-cell patch-clamp recordings were made in coronal slices (250 μm) containing the medial habenula from Wt and transgenic mice (P7-P14). Acute brain slices were cut with a vibratome (Microm HM 650 V) and kept in ice cold oxygenated (95 % O_2 and 5 % CO_2) artificial cerebrospinal fluid (ACSF) containing (mM): 125 NaCl, 2.5 KCl, 1.3 $MgCl_2$, 2 $CaCl_2$, 1.25 KH_2PO_4, 11 glucose, 26 $NaHCO_3$, pH 7.4, osmolarity 310 and allowed to recover for at least one hour in oxygenated ACSF at RT. The recording chamber was gravity fed with the same buffer. Habenula neurons were visually identified with a microscope (Axioskop 2 FS plus) equipped with a digital camera (SPOT Insight). Patch electrodes were made from borosilicate glass (1B150F-4, World Precision Instruments, Inc.) with a microelectrode puller (P-97, Sutter Instrument CO). The internal pipette solution contained (mM): 130 KCl, 2 $MgCl_2$, 0.5 $CaCl_2$, 5 EGTA, 10 HEPES, pH 7.3, osmolarity 280 (resistance 5-7 MΩ). Typical series resistance was 15-30 MΩ. Nicotine was locally applied (50 ms, 18-10 psi) at different concentrations (1 – 600 μM) with a pressure device (PR-10, ALA Scientific Instruments) connected to a focal perfusion system (VM4, ALA Scientific Instruments) controlled with a trigger interface (TIB 14S, HEKA). The pipette was moved within 15-20 μm of the recorded cell with a motorized micromanipulator (LN mini 25, control system SM-5, Luigs & Neumann) for drug application and retracted after the end of the puff to minimize desensitization. In current clamp the pipette with nicotine was positioned 100 μm from the cell and the drug was applied for 3 s. Neurons showing spontaneous oscillations were not tested. Currents were recorded with a HEKA amplifier (EPC 10) using PatchMaster software (V2.20, HEKA), and analyzed with FitMaster software (V2.3, HEKA). Membrane potential was hold at -70 mV. Dose-response curves were calculated relative to the maximal response to nicotine (*n* = 3 cells per genotype).

Receptor ligand autoradiography. Adult brains were dissected and immediately embedded in O.C.T. compound (Sakura). Frozen tissues were cut at the cryostat (20 μm coronal sections), thaw mounted on ultra frost microscope slides (Menzel Gläser) and stored at -80 °C. For total [125I]-epibatidine binding sites, sections of Wt and transgenic littermates (*n* = 3 per genotype) were incubated with 200 pM [125I]-epibatidine (NEN Perkin Elmer, Boston; specific activity 2200

Ci/mmole) in Tris 50mM pH 7.4 for 1 hour. For cytisine-resistant [125I]-epibatidine binding sites, sections were first incubated with 25mM Cytisine (Sigma- St Louis) in Tris 50mM PH 7.4 for 30 min, as described previously (Zoli et al., 1995). Quantification of binding was done with ImageJ (NIH).

Oral nicotine consumption: no-choice paradigm. Wt (*n* = 5) and Tabac (*n* = 5) male mice were single-housed in their home cage. Mice were provided with either nicotine or saccharin solutions as their sole source of fluid and bottles were weighed daily to measure nicotine intake. The volume of the drinking solution consumed per day was averaged for the period of consumption (3 days). Drinking solutions were: water, 2% saccharine in water (sweet water), 5mM Quinine (bitter water) or 100 μM nicotine in sweet water. Nicotine tartrate was dissolved in 0.9% sterile saline (all concentrations of nicotine refer to the free base form). The dose consumed was calculated as the milligrams of nicotine consumed per day considering the body weight of the mouse (mg/kg/d).

Oral nicotine consumption: free-choice paradigm. Voluntary nicotine intake was assessed in adult male Wt (*n* = 7) and Tabac (*n* = 6) mice, using the 2-bottle assay as described before (Butt et al., 2005). Naïve mice were presented with 2 bottles of water in the home cage for acclimatization to the new conditions for the first 3 days of testing. After this period, one of the bottles was filled with a nicotine solution (1 μg/ml) diluted in water. The intake of fluid from each bottle was measured daily for 3 days. The concentration of the nicotine solution was then increased and tested for another 3 days. In total, 6 different concentrations were tested consecutively (1, 5, 12.5, 25, 50 and 100 μg/ml). Percent of nicotine consumption was expressed as a ratio of the volume of nicotine solution consumed divided by the total fluid intake (ml nicotine x 100% / ml total).

Conditioned place aversion. The apparatus used was a rectangular box composed of three distinct compartments separated by removable doors. The center compartment (10 x 20 x 10 cm) is grey with a polycarbonate smooth floor. The choice compartments (20 x 40 x 20 cm) have

different visual and tactile cues. One choice compartment has black walls with a 0.75 cm stainless steel mesh floor. The other compartment has white walls with a 0.25 cm stainless steel mesh floor. Behavior of animals was videotaped and scored by a blind observer. Preconditioning phase: On day 1, mice (8-12 weeks old) were allowed to explore the three compartments freely for 15 min. This preconditioning session was used to separate mice into groups with approximately equal biases for each side. None of the mice exhibited a strong preference for one side over the other. Conditioning phase: During the following three days, two pairings per day were given at 4-5 h apart. The doors between the compartments were closed so that animals were confined to one side or the other of the conditioning box for 15 min. In the morning the animals were given an IP saline injection prior to the placement in the chamber. In the afternoon, animals received a nicotine injection (IP, 0.5 mg/kg) prior to the placement in the opposing chamber. Preference test: On day 5, the doors between the compartments were opened again. Mice were placed in the central chamber and were allowed to move freely in the three chambers for 15 min. Time spent on each side was recorded.

Lentivirus production. Recombinant lentiviral vectors were prepared using transient transfection of HEK293T cells. Briefly, 5×10^6 HEK293T cells were seeded on 24 × 10 cm cell-culture dishes pre-coated with poly-L-lysine (Sigma-Aldrich). The next day, the transfer vector plus the packaging vectors pLP1 and pLP2 (ViraPower System; Invitrogen) and the envelope vector pCMV-VSV-G (Addgene) were cotransfected with PEI transfection (Polyethylenimine MAX, Polysciences Inc.) into HEK293T cells. The transfection mix was prepared as follows (for one dish): 12 µg transfer plasmid, 6.5 µg pLP1, 3.5 µg pLP2 and 3.5 µg pCMV-VSV-G were added to 800 µl OptiMEM (Gibco) and incubated at RT for 5 min. In the meanwhile, 51 µl PEI solution (1 mg/ml) was added to 800 µl OptiMEM in a separate tube. Both solutions were mixed and incubated at RT for 30 min. During the incubation time, the medium of the cells was changed to 5 ml OptiMEM per dish. Finally, 3 ml transfection mix was added to each dish. After 7-8 h, the medium was replaced by 9 ml OptiMEM per dish, without addition of FBS. The virus containing medium was harvested 40–45 h after medium change, cleared by centrifugation at 2,500 g for 10

min at 4 °C and filtered through 0.45 µm filter units (Millipore). Virus concentration was carried out by ultracentrifugation in a Beckman Optima L-90K ultracentrifuge using a SW32 Ti rotor at 50,000 *g* for 3 h with a purification layer of 1 ml 20% sucrose (in dH_20) added to the bottom of the centrifuge tubes. Subsequently, the virus was resuspended in 50-100 µl 1x PBS, aliquoted and stored at -70 °C. The titer of concentrated lentivirus was determined by transducing 1×10^5 HEK293T cells per well in a 24 well cell culture plate with limiting virus dilutions and quantification of GFP positive cells by FACS analysis after 3 d. Titers of concentrated lentivirus were in the range of $5 \times 10^8 – 2 \times 10^9$ TU ml^{-1}.

Stereotaxic injections. Tabac mice, aged 8–13 weeks, were anesthetized with ketamine and xylazine (130 and 10 mg kg^{-1}) and placed in a Benchmark stereotaxic frame with a Cunningham mouse adaptor. 0.5 µl of virus was injected bilaterally with a pulled glass pipette (flow rate 0.1 µl min^{-1}) into the medial habenula at the following coordinates: antero-posterior (from bregma): –1.4 mm and –1.75 mm; lateral +/-0.36 mm and dorso-ventral (from skull level) –2.7 mm and –2.72 mm. Behavioral experiments started 2 weeks after injections. Verification of the injection sites was done on brain sections immunostained with rabbit polyclonal anti-RFP (Molecular Probes) diluted 1:1000.

Statistical Analysis. Unpaired two-tailed Student t-tests were used for analyzing most of the data, except when two-way analysis of variance with Anova or paired two-tailed Student t-tests are indicated. Results are presented as means ± SEM.

ACKNOWLEDGMENTS

We thank J. Xing (Rockefeller University, New York, NY), S. Wojtke, B. Kampfrath and J. Reiche (MDC, Germany) for technical support. J. Stitzel for mouse nAChR clones (University of

Colorado, Boulder, CO), W. Kummer (University of Giessen, Germany), G. Lewin (MDC, Germany), C. Birchmeier (MDC, Germany) and M. Andrade (MDC, Germany) for helpful discussions, A. Garratt (MDC, Germany) for providing the SP antibody and F. Rathjen (MDC, Germany) for the CD28 antibody. This work was supported by the Helmholtz Association 31-002, the Sonderforschungsbereich SFB 665, the Deutsche Forschungsgemeinschaft DFG RA 424/5-1, by MCB RAS and RFBR.

REFERENCES:

Amos, C.I., Gorlov, I.P., Dong, Q., Wu, X., Zhang, H., Lu, E.Y., Scheet, P., Greisinger, A.J., Mills, G.B., and Spitz, M.R. (2010a). Nicotinic acetylcholine receptor region on chromosome 15q25 and lung cancer risk among African Americans: a case-control study. J Natl Cancer Inst *102*, 1199-1205.

Amos, C.I., Spitz, M.R., and Cinciripini, P. (2010b). Chipping away at the genetics of smoking behavior. Nat Genet *42*, 366-368.

Auer S., Stuerzebecher A.S., Juettner R., Santos-Torres J., Hanack C., Frahm S., Liehl B. and Ibanez-Tallon I. (2010). Silencing neurotransmission with membrane-tethered toxins. Nat Methods *7*, 229-36.

Bacher, I., Wu, B., Shytle, D.R., and George, T.P. (2009). Mecamylamine - a nicotinic acetylcholine receptor antagonist with potential for the treatment of neuropsychiatric disorders. Expert Opin Pharmacother *10*, 2709-2721.

Bierut, L.J. (2010). Convergence of genetic findings for nicotine dependence and smoking related diseases with chromosome 15q24-25. Trends Pharmacol Sci *31*, 46-51.

Bierut, L.J., Stitzel, J.A., Wang, J.C., Hinrichs, A.L., Grucza, R.A., Xuei, X., Saccone, N.L., Saccone, S.F., Bertelsen, S., Fox, L.*, et al.* (2008). Variants in nicotinic receptors and risk for nicotine dependence. Am J Psychiatry *165*, 1163-1171.

Bigger, C.B., Melnikova, I.N., and Gardner, P.D. (1997). Sp1 and Sp3 regulate expression of the neuronal nicotinic acetylcholine receptor beta4 subunit gene. J Biol Chem *272*, 25976-25982.

Butt C.M., King N.M., Hutton S.R., Collins A.C. and Stitzel J.A. (2005). Modulation of nicotine but not ethanol preference by the mouse Chrna4 A529T polymorphism. Behav Neurosci*. 199*, 26-37.

Carland, J.E., Cooper, M.A., Sugiharto, S., Jeong, H.J., Lewis, T.M., Barry, P.H., Peters, J.A., Lambert, J.J., and Moorhouse, A.J. (2009). Characterization of the effects of charged residues in the intracellular loop on ion permeation in alpha1 glycine receptor channels. J Biol Chem *284*, 2023-2030.

Changeux, J.P. (2010). Nicotine addiction and nicotinic receptors: lessons from genetically modified mice. Nat Rev Neurosci *11*, 389-401.

Dani, J.A., and Heinemann, S. (1996). Molecular and cellular aspects of nicotine abuse. Neuron *16*, 905-908.

De Biasi, M., and Salas, R. (2008). Influence of neuronal nicotinic receptors over nicotine addiction and withdrawal. Exp Biol Med (Maywood) *233*, 917-929.

Dineley-Miller, K., and Patrick, J. (1992). Gene transcripts for the nicotinic acetylcholine receptor subunit, beta4, are distributed in multiple areas of the rat central nervous system. Brain Res Mol Brain Res *16*, 339-344.

Flora, A., Schulz, R., Benfante, R., Battaglioli, E., Terzano, S., Clementi, F., and Fornasari, D. (2000). Transcriptional regulation of the human alpha5 nicotinic receptor subunit gene in neuronal and non-neuronal tissues. Eur J Pharmacol *393*, 85-95.

Fowler C.D, Lu Q., Johnson P.M., Marks M.J., and Kenny P.J. (2011). Habenular α5 nicotinic receptor subunit signalling controls nicotine intake. Nature Jan 30. [Epub ahead of print]

Gahring, L.C., and Rogers, S.W. (2010). Nicotinic receptor subunit alpha5 modifies assembly, up-regulation, and response to pro-inflammatory cytokines. J Biol Chem *285*, 26049-26057.

Glatt, A.R., Denton, K., and Boughter, J.D., Jr. (2009). Variation in nicotine consumption in inbred mice is not linked to orosensory ability. Chem Senses *34*, 27-35.

Gong, S., Zheng, C., Doughty, M.L., Losos, K., Didkovsky, N., Schambra, U.B., Nowak, N.J., Joyner, A., Leblanc, G., Hatten, M.E., and Heintz, N. (2003). A gene expression atlas of the central nervous system based on bacterial artificial chromosomes. Nature *425*, 917-925.

Gotti, C., Clementi, F., Fornari, A., Gaimarri, A., Guiducci, S., Manfredi, I., Moretti, M., Pedrazzi, P., Pucci, L., and Zoli, M. (2009). Structural and functional diversity of native brain neuronal nicotinic receptors. Biochem Pharmacol *78*, 703-711.

Grady S.R., Moretti M., Zoli M., Marks M.J., Zanardi A., Pucci L., Clementi F., and Gotti C. (2009) Rodent habenulo-interpeduncular pathway expresses a large variety of uncommon nAChR subtypes, but only the alpha3beta4* and alpha3beta3beta4* subtypes mediate acetylcholine release. J Neurosci*. 29*, 2272-82.

Ibañez-Tallon I., Miwa J.M., Wang H.L., Adams N.C., Crabtree G.W., Sine S.M. and Heintz N. (2002). Novel modulation of neuronal nicotinic acetylcholine receptors by association with the endogenous prototoxin lynx1. Neuron *33*, 893-903.

Ikemoto, S., Qin, M., and Liu, Z.H. (2006). Primary reinforcing effects of nicotine are triggered from multiple regions both inside and outside the ventral tegmental area. J Neurosci *26*, 723-730.

Jackson, K.J., Martin, B.R., Changeux, J.P., and Damaj, M.I. (2008). Differential role of nicotinic acetylcholine receptor subunits in physical and affective nicotine withdrawal signs. J Pharmacol Exp Ther *325*, 302-312.

Kedmi, M., Beaudet, A.L., and Orr-Urtreger, A. (2004). Mice lacking neuronal nicotinic acetylcholine receptor beta4-subunit and mice lacking both alpha5- and beta4-subunits are highly resistant to nicotine-induced seizures. Physiol Genomics *17*, 221-229.

Kelley, S.P., Dunlop, J.I., Kirkness, E.F., Lambert, J.J., and Peters, J.A. (2003). A cytoplasmic region determines single-channel conductance in 5-HT3 receptors. Nature *424*, 321-324.

Lee, Y., Rudell, J., and Ferns, M. (2009). Rapsyn interacts with the muscle acetylcholine receptor via alpha-helical domains in the alpha, beta, and epsilon subunit intracellular loops. Neuroscience *163*, 222-232.

Levitin, F., Weiss, M., Hahn, Y., Stern, O., Papke, R.L., Matusik, R., Nandana, S.R., Ziv, R., Pichinuk, E., Salame, S*., et al.* (2008). PATE gene clusters code for multiple, secreted TFP/Ly-6/uPAR proteins that are expressed in reproductive and neuron-rich tissues and possess neuromodulatory activity. J Biol Chem *283*, 16928-16939.

Lu, B., Su, Y., Das, S., Wang, H., Wang, Y., Liu, J., and Ren, D. (2009). Peptide neurotransmitters activate a cation channel complex of NALCN and UNC-80. Nature *457*, 741-744.

Marks, M.J., Laverty, D.S., Whiteaker, P., Salminen, O., Grady, S.R., McIntosh, J.M., and Collins, A.C. (2010). John Daly's compound, epibatidine, facilitates identification of nicotinic receptor subtypes. J Mol Neurosci *40*, 96-104.

Maskos, U. (2008). The cholinergic mesopontine tegmentum is a relatively neglected nicotinic master modulator of the dopaminergic system: relevance to drugs of abuse and pathology. Br J Pharmacol *153 Suppl 1*, S438-445.

Maskos, U., Molles, B.E., Pons, S., Besson, M., Guiard, B.P., Guilloux, J.P., Evrard, A., Cazala, P., Cormier, A., Mameli-Engvall, M*., et al.* (2005). Nicotine reinforcement and cognition restored by targeted expression of nicotinic receptors. Nature *436*, 103-107.

McGehee, D.S., and Role, L.W. (1995). Physiological diversity of nicotinic acetylcholine receptors expressed by vertebrate neurons. Annu Rev Physiol *57*, 521-546.

McGehee D.S., Heath M.J., Gelber S., Devay P., Role L.W. (1995). Nicotine enhancement of fast excitatory synaptic transmission in CNS by presynaptic receptors Science. 269:1692-6

Medel, Y.F., and Gardner, P.D. (2007). Transcriptional repression by a conserved intronic sequence in the nicotinic receptor alpha3 subunit gene. J Biol Chem *282*, 19062-19070.
Meliska, C.J., Bartke, A., McGlacken, G., and Jensen, R.A. (1995). Ethanol, nicotine, amphetamine, and aspartame consumption and preferences in C57BL/6 and DBA/2 mice. Pharmacol Biochem Behav *50*, 619-626.
Nashmi, R., Dickinson, M.E., McKinney, S., Jareb, M., Labarca, C., Fraser, S.E., and Lester, H.A. (2003). Assembly of alpha4beta2 nicotinic acetylcholine receptors assessed with functional fluorescently labeled subunits: effects of localization, trafficking, and nicotine-induced upregulation in clonal mammalian cells and in cultured midbrain neurons. J Neurosci *23*, 11554-11567.
O'Dell, L.E., and Khroyan, T.V. (2009). Rodent models of nicotine reward: what do they tell us about tobacco abuse in humans? Pharmacol Biochem Behav *91*, 481-488.
Perry, D.C., and Kellar, K.J. (1995). [3H]epibatidine labels nicotinic receptors in rat brain: an autoradiographic study. J Pharmacol Exp Ther *275*, 1030-1034.
Picciotto, M.R. (1998). Common aspects of the action of nicotine and other drugs of abuse. Drug Alcohol Depend *51*, 165-172.
Quick, M.W., Ceballos, R.M., Kasten, M., McIntosh, J.M., and Lester, R.A. (1999). Alpha3beta4 subunit-containing nicotinic receptors dominate function in rat medial habenula neurons. Neuropharmacology *38*, 769-783.
Ren, X.Q., Cheng, S.B., Treuil, M.W., Mukherjee, J., Rao, J., Braunewell, K.H., Lindstrom, J.M., and Anand, R. (2005). Structural determinants of alpha4beta2 nicotinic acetylcholine receptor trafficking. J Neurosci *25*, 6676-6686.
Rezvani, K., Teng, Y., and De Biasi, M. (2010). The ubiquitin-proteasome system regulates the stability of neuronal nicotinic acetylcholine receptors. J Mol Neurosci *40*, 177-184.
Robinson, S.F., Marks, M.J., and Collins, A.C. (1996). Inbred mouse strains vary in oral self-selection of nicotine. Psychopharmacology (Berl) *124*, 332-339.
Rose, J.E. (2007). Multiple brain pathways and receptors underlying tobacco addiction. Biochem Pharmacol *74*, 1263-1270.
Saccone, N.L., Wang, J.C., Breslau, N., Johnson, E.O., Hatsukami, D., Saccone, S.F., Grucza, R.A., Sun, L., Duan, W., Budde, J.*, et al.* (2009). The CHRNA5-CHRNA3-CHRNB4 nicotinic receptor subunit gene cluster affects risk for nicotine dependence in African-Americans and in European-Americans. Cancer Res *69*, 6848-6856.
Salas, R., Pieri, F., and De Biasi, M. (2004). Decreased signs of nicotine withdrawal in mice null for the beta4 nicotinic acetylcholine receptor subunit. J Neurosci *24*, 10035-10039.
Salas, R., Sturm, R., Boulter, J., and De Biasi, M. (2009). Nicotinic receptors in the habenulo-interpeduncular system are necessary for nicotine withdrawal in mice. J Neurosci *29*, 3014-3018.
Scofield, M.D., Tapper, A.R., and Gardner, P.D. (2010). A transcriptional regulatory element critical for CHRNB4 promoter activity in vivo. Neuroscience *170*, 1056-1064.
Stuerzebecher A.S., Hu J., Smith E.S., Frahm S., Santos-Torres J., Kampfrath B., Auer S., Lewin G.R. and Ibanez-Tallon I. (2010). An in vivo tethered toxin approach for the cell-autonomous inactivation of voltage-gated sodium channel currents in nociceptors. J Physiol. *588*, 1695-707.
Tapper, A.R., McKinney, S.L., Nashmi, R., Schwarz, J., Deshpande, P., Labarca, C., Whiteaker, P., Marks, M.J., Collins, A.C., and Lester, H.A. (2004). Nicotine activation of alpha4* receptors: sufficient for reward, tolerance, and sensitization. Science *306*, 1029-1032.
Taraschenko, O.D., Shulan, J.M., Maisonneuve, I.M., and Glick, S.D. (2007). 18-MC acts in the medial habenula and interpeduncular nucleus to attenuate dopamine sensitization to morphine in the nucleus accumbens. Synapse *61*, 547-560.
Thorgeirsson, T.E., Geller, F., Sulem, P., Rafnar, T., Wiste, A., Magnusson, K.P., Manolescu, A., Thorleifsson, G., Stefansson, H., Ingason, A.*, et al.* (2008). A variant associated with nicotine dependence, lung cancer and peripheral arterial disease. Nature *452*, 638-642.
Unwin, N. (2005). Refined structure of the nicotinic acetylcholine receptor at 4A resolution. J Mol Biol *346*, 967-989.
Weiss, R.B., Baker, T.B., Cannon, D.S., von Niederhausern, A., Dunn, D.M., Matsunami, N., Singh, N.A., Baird, L., Coon, H., McMahon, W.M.*, et al.* (2008). A candidate gene approach

identifies the CHRNA5-A3-B4 region as a risk factor for age-dependent nicotine addiction. PLoS Genet *4*, e1000125.
Whiting, P.J., and Lindstrom, J.M. (1988). Characterization of bovine and human neuronal nicotinic acetylcholine receptors using monoclonal antibodies. J Neurosci *8*, 3395-3404.
Xu, W., Gelber, S., Orr-Urtreger, A., Armstrong, D., Lewis, R.A., Ou, C.N., Patrick, J., Role, L., De Biasi, M., and Beaudet, A.L. (1999). Megacystis, mydriasis, and ion channel defect in mice lacking the alpha3 neuronal nicotinic acetylcholine receptor. Proc Natl Acad Sci U S A *96*, 5746-5751.
Xu, X., Scott, M.M., and Deneris, E.S. (2006). Shared long-range regulatory elements coordinate expression of a gene cluster encoding nicotinic receptor heteromeric subtypes. Mol Cell Biol *26*, 5636-5649.
Yang, K., Hu, J., Lucero, L., Liu, Q., Zheng, C., Zhen, X., Jin, G., Lukas, R.J., and Wu, J. (2009). Distinctive nicotinic acetylcholine receptor functional phenotypes of rat ventral tegmental area dopaminergic neurons. J Physiol *587*, 345-361.
Zoli, M., Le Novere, N., Hill, J.A., Jr., and Changeux, J.P. (1995). Developmental regulation of nicotinic ACh receptor subunit mRNAs in the rat central and peripheral nervous systems. J Neurosci *15*, 1912-1939.
Zoli, M., Lena, C., Picciotto, M.R., and Changeux, J.P. (1998). Identification of four classes of brain nicotinic receptors using beta2 mutant mice. J Neurosci *18*, 4461-4472.

FIGURE LEGENDS

Figure 1. Increase of nAChR currents by β4 is competed by α5 and maps to a single amino acid (S435)

(A) Quantification of nicotine-evoked currents (100 μM, 20 s) recorded in *Xenopus* oocytes injected with mouse α3:β2, α3:β4 and α3:β4:α5 cRNAs at the indicated ratios. Current amplitudes from 1:3 to 1:10 α3β4 combinations are significantly increased compared to 1:1 ratio (**P* < 0.05 and ****P* < 0.001). Addition of α5 to the α3β4 complex leads to significant decrease of current amplitudes when equal amounts of β4 and α5 are injected (***P* < 0.01 for Wt α5 and ****P* < 0.001 for α5 D397N). The D397N variant shows significantly stronger competition with β4 compared to Wt α5 (**P* < 0.05). Triangles indicate increasing relative amounts of one specified subunit.

(B) Representative traces of two-electrode-voltage-clamp recordings.

(C) Schematic representation of β2/β4 chimeras indicating the domains, motifs or residues exchanged between β4 (in green) and β2 (in black) subunits and corresponding aminoacid number and substitutions (left). Fold current increase (right) indicates the relative current

amplitude of nicotine-evoked currents for each β2/β4 chimera expressed with the α3 subunit at 1:10 relative to 1:1. All values are expressed as mean ± s.e.m.; *n* = 5 per ratio in all experiments.

Figure 2. Electrostatic mapping of the intracellular vestibule of the α3β4α5 nAChR complex

(A) Alignment of human (HS), mouse (MM) and torpedo (TC) sequences spanning the MA-stretch of the indicated nAChR subunits. The S435 residue in β4 and the D397 residue in α5 are indicated by a black frame.

(B) Model of the three-dimensional structure of the $\alpha3_2\beta4_2\alpha5_1$ nAChR. Transmembrane and intracellular domains of α3, α5 and β4 subunits are shown in orange, red and green, respectively. EC extracellular space; IC intracellular space. The indicated S435 residue in β4 and the D397 residue in α5 are located at the tip of the intracellular vestibule.

(C) Electrostatic potential surface representations showing frontal (upper panel) and back (lower panel) views of the intracellular vestibule formed by the $\alpha3_2\beta4_2\alpha5_1$ nAChR. One α3 subunit and one β4 subunit are removed for visualization of the cavity. Horizontal gray bar indicate the plasma membrane. The electrostatic surface was contoured between -15kT/e and +15kT/e; negative and positive charges are marked in red and blue, respectively. Residues corresponding to the β4-potentiating residue S435 and D397 in α5 are indicated.

Figure 3. Tabac mice express elevated *Chrnb4* transcripts in *Chrna3*-eGFP labeled neurons

(A) Scheme of the modified mouse BAC containing the *Chrnb4-Chrna3-Chrna5* gene cluster. Yellow boxes: exons, green box: eGFP cassette, white box: polyadenylation signal (pA), black arrows: direction of transcription, red crosses: truncated transcription, *cis*-regulatory elements marked in red: conserved non-coding region (CNR4), β43' enhancer (Xu et al., 2006), E1/E2: SP1 and SP3 binding sites (Bigger et al., 1997) and α3-i: transcriptional silencer (Medel and Gardner, 2007).

(B) Western blot analyses of β4 (53 kD), α5 (2 splice variants: 50 kD and 53 kD) and α-tubulin in brain extracts of Wt and Tabac mice.

(C-H) EGFP expressing neurons (green) in peripheral SCG (C) and in sagittal brain sections (except G: coronal) of Tabac mice immunostained with TH (D and E) and ChAT (F-H) in red. Scale bars: (C) 100 μm; (D-F) 500 μm (magnification of D is indicated by the dotted lines, scale bar 50 μm); (G) 50 μm and (H) 250 μm.

(I and J) *In situ* hybridization of *Chrnb4* transcripts in Wt and Tabac brain sections. Scale bars: MHb 100 μm; SuM 50 μm; IPN 250 μm; VTA 100 μm.

Abbreviations: tyrosine hydroxylase (TH), choline acetyltransferase (ChAT), medial habenula (MHb), fasciculus retroflexus (fr), ventral tegmental area (VTA), periaqueductal gray (pAg), caudal linear nucleus (Cli), supramammilary nucleus (SuM), interpeduncular nucleus (IPN), laterodorsal tegmentum (LdT), substantia nigra (SN), superior cervical ganglia (SCG).

Figure 4. Tabac mice show increased α3β4* nAChR nicotine-evoked currents and firing frequency in *Chrna3*-eGFP labeled neurons

(A-F) Whole cell patch clamp recordings of MHb neurons in acute brain slices from Wt and Tabac mice. Representative traces of nicotine-evoked currents (A: 100 μM, 50 ms application) and corresponding concentration-response relationships (B: peak amplitudes ± s.e.m, n = 5-8 cells per genotype, $P < 0.05$ by two-way anova). Dose-response curves in C were calculated relative to the maximal response to nicotine from B. Mecamylamine (D: MEC, 3 μM, 3 min) inhibition of nicotine-evoked currents in neurons of Tabac mice. Representative current clamp recordings (E) and quantification of action potentials upon local application of nicotine (1 μM, 3 s) in neurons of Wt and Tabac mice (F: mean firing frequency ± s.e.m., n = 4, $P < 0.01$). Numbers in parenthesis represent number of neurons tested. All values are expressed as mean ± s.e.m.

Figure 5. Increased number of α3β4* nAChR binding sites in Tabac mice

(A and B) Film autoradiograms of [^{125}I] epibatidine binding to α3β4* and α4β2* sites in Wt (A) and Tabac (B) coronal brain sections.

(C and D) Detection of $\alpha 3\beta 4$* sites (arrows) by competition of [^{125}I] epibatidine binding with unlabeled cytisine.

(E) Direct fluorescence (green) of *Chrna3*/eGFP positive cell populations and immunostaining of coronal brain sections from Tabac mice with the indicated antibodies (red: TH, NeuN, Substance P (SP) and CD28). Scale bars from top to bottom are 50, 25, 50, 25, 250 and 50 µm. Same abbreviations as in Figure 1, and mitral cells (Mi), granule layer (Gl) accessory olfactory bulb (aOB), medial preoptic area (mPO), primary sensory cortex layer IV (S1), piriform cortex (Pir), hippocampus (Hip), amygdala (Am), subthalamic nucleus (STh), superior colliculus (sc), paramedian raphe nucleus (PMR), cerebellum (Cb), basket cells (arrow), parallel fibers (insert), nucleus raphe magnus (RMg) and medial vestibular nucleus (MVe).

Figure 6. Tabac mice consume less nicotine and show conditioned place aversion

(A and B) Nicotine consumption in a no-choice paradigm (1 drinking bottle). (A) Drinking volumes (ml/mouse/day) of water, sweet water (2% saccharine) and bitter water (5 mM quinine). The tested period of consumption was 3 days (# paired t-test, $P < 0.05$). (B) The dose of nicotine consumed expressed as the milligrams of nicotine consumed per day considering the body weight of the mouse (mg/kg/d) ($P < 0.05$). Wt: $n = 10$, Tabac: $n = 10$.

(C) Nicotine consumption in a two-bottle-choice paradigm between water and water containing the indicated nicotine concentrations expressed as percent of the volume of nicotine solution consumed divided by the total fluid intake and per day. Each concentration was tested for 3 days. Dashed line at 50 % indicates no preference. Wt mice ($n = 7$) Tabac mice ($n = 6$); Two way anova: $P < 0.05$.

(D) Body weight of Wt and Tabac mice after nicotine drinking tests.

(E) Nicotine administration (0.5 mg/kg) elicits place aversion to nicotine-paired environment in Tabac mice. Following conditioning, Tabac mice preferred the saline-paired environment over the nicotine-paired environment (paired t-test, #$P < 0.05$). Wt mice spent significantly more time in the nicotine paired environement compared to Tabac mice (*$P < 0.05$) (Wt mice $n = 7$ Tabac mice $n =$

6). Data are expressed as time spent in drug-paired environments after drug conditioning. All values are expressed as mean ± s.e.m.

Figure 7. Reversal of nicotine aversion in Tabac mice by lentiviral-mediated expression of the α5 D397N variant in the MHb

(A) Schematic representation of the lentiviral (LV) constructs used for brain stereotactic injections. LV-α5N carries the mouse α5 variant D397N followed by an IRES and the mCHERRY reporter. The control virus (LV-PC) carries mCHERRY fused to the N-terminus of the transmembrane domain of the PDGF receptor (TM-PDGF) via a linker domain.

(B) Coronal brain sections of Tabac mice stereotactically injected in the MHb with the indicated lentivirus. Colocalization of eGFP fluorescence driven by the transgene in Tabac mice and mCherry red fluorescence for LV-PC or mCherry immnofluorescence for LV-α5N injected mice. Scale bars: 100 μm.

(C and D) Two-bottle choice nicotine consumption in Tabac mice after stereotactic bilateral injection of control (LV-PC) and mutated α5 (LV-α5N) lentiviral constructs in the MHb. Tabac mice backcrossed to C57BL6, $n = 4$ for LV-PC and $n = 5$ for LV-α5N, $P < 0.05$ (C) and Tabac mice hybrid of FVB/N and Swiss Webster, $n = 8$ for LV-PC and $n = 9$ for LV-α5N (D).

Figure 1

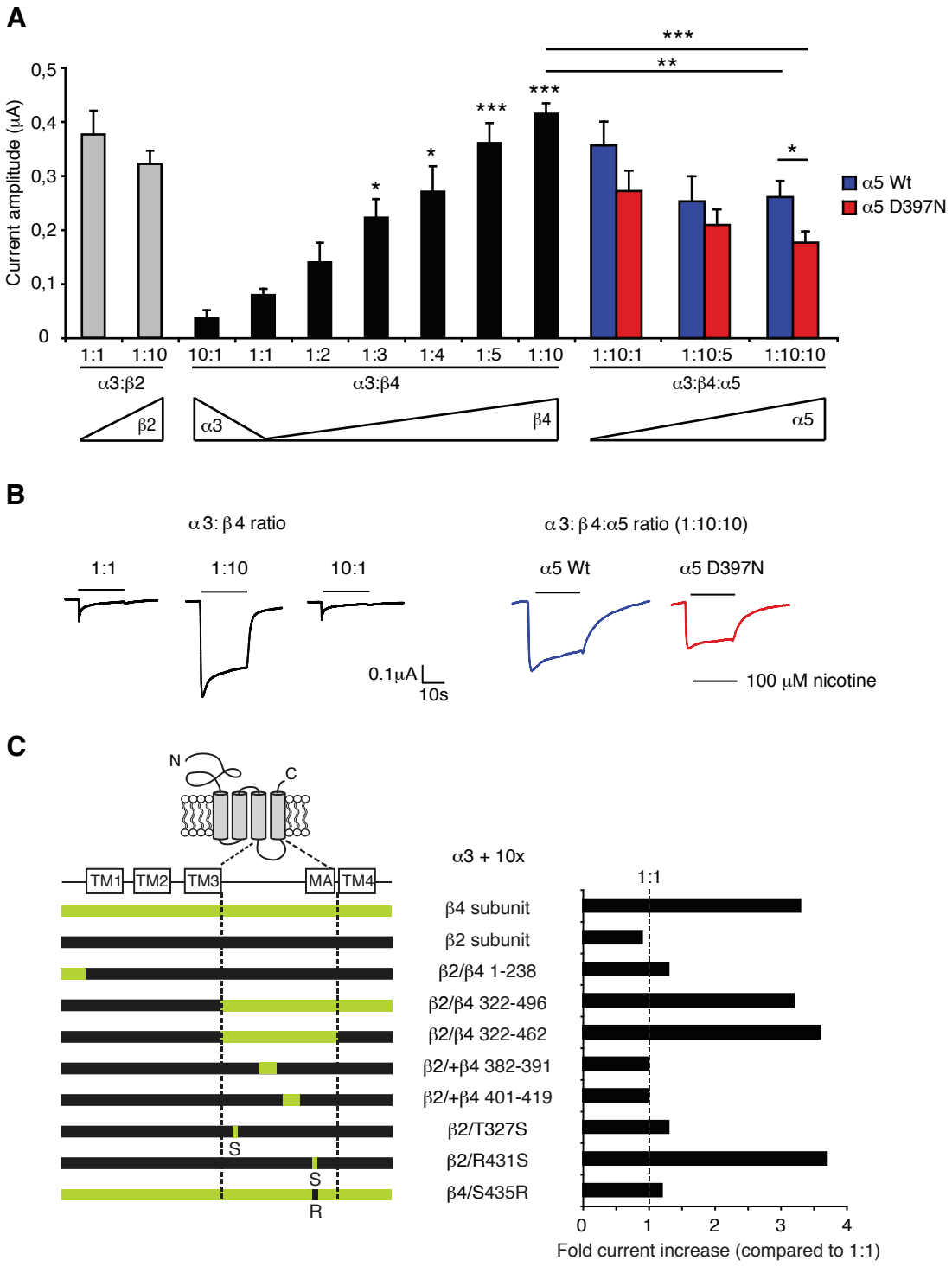
A
Current amplitude (μA)
0,5
0,4
0,3
0,2
0,1
0
***
**
***
***
*
*
*
*
α5 Wt
α5 D397N
1:1
1:10
10:1
1:1
1:2
1:3
1:4
1:5
1:10
1:10:1
1:10:5
1:10:10
α3:β2
α3:β4
α3:β4:α5
β2
α3
β4
α5
B
α3:β4 ratio
α3:β4:α5 ratio (1:10:10)
1:1
1:10
10:1
α5 Wt
α5 D397N
0.1μA
10s
100 μM nicotine
C
N
C
TM1
TM2
TM3
MA
TM4
S
S
R
α3 + 10x
1:1
β4 subunit
β2 subunit
β2/β4 1-238
β2/β4 322-496
β2/β4 322-462
β2/+β4 382-391
β2/+β4 401-419
β2/T327S
β2/R431S
β4/S435R
0
1
2
3
4
Fold current increase (compared to 1:1)

Figure 2

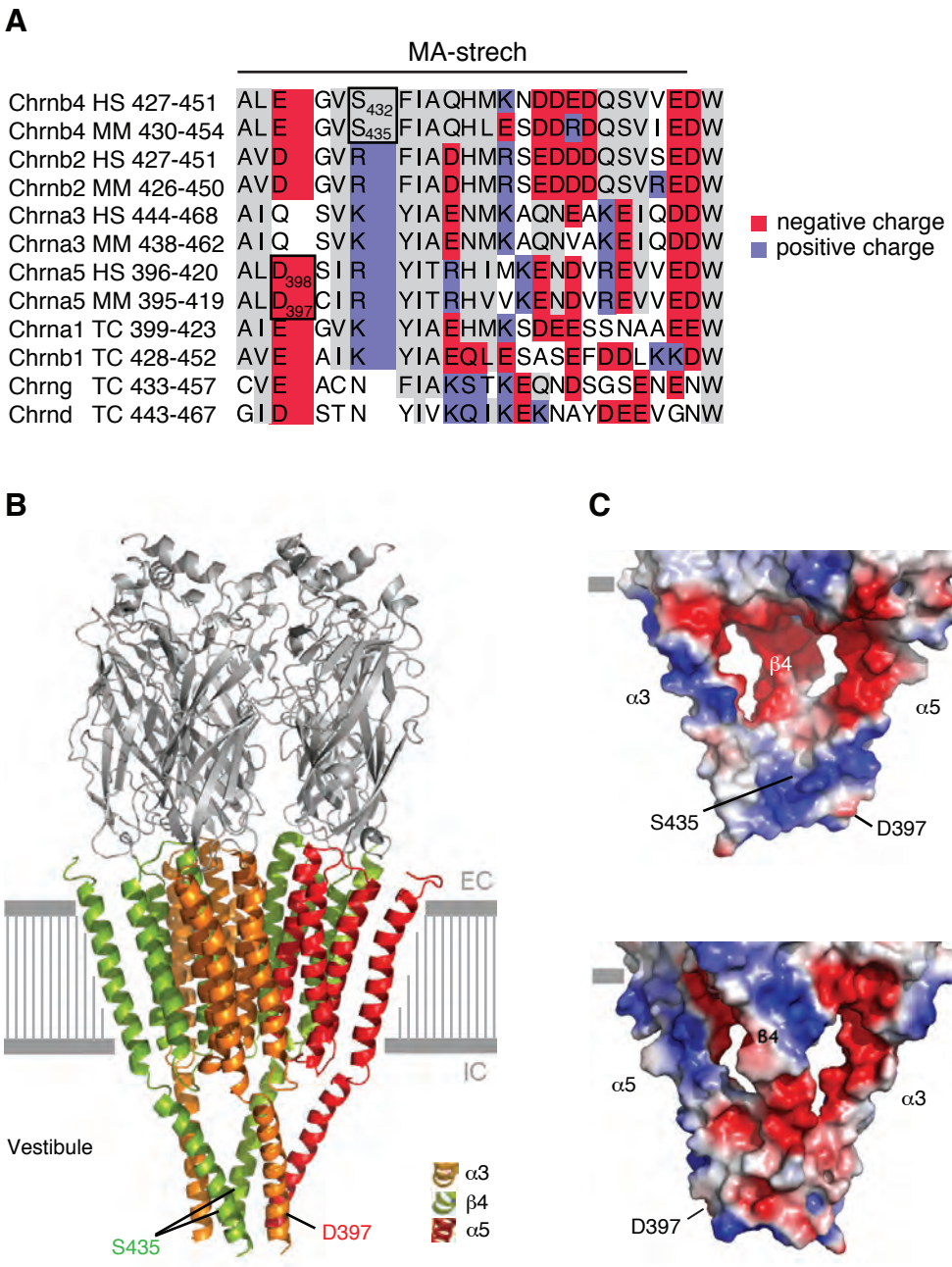
A
MA-strech
Chrnb4 HS 427-451 ALE GVS432 FIAQHMKNDDEDQSVVEDW
Chrnb4 MM 430-454 ALE GVS435 FIAQHLESDDRDQSVIEDW
Chrnb2 HS 427-451 AVD GVR FIADHMRSEDDDQSVSEDW
Chrnb2 MM 426-450 AVD GVR FIADHMRSEDDDQSVREDW
Chrna3 HS 444-468 AIQ SVK YIAENMKAQNEAKEIQDDW
Chrna3 MM 438-462 AIQ SVK YIAENMKAQNVAKEIQDDW
Chrna5 HS 396-420 ALD398 SIR YITRHIMKENDVREVVEDW
Chrna5 MM 395-419 ALD397 CIR YITRHVVKENDVREVVEDW
Chrna1 TC 399-423 AIE GVK YIAEHMKSDEESSNAAEEW
Chrnb1 TC 428-452 AVE AIK YIAEQLESASEFDDLKKDW
Chrng TC 433-457 CVE ACN FIAKSTKEQNDSGSENENW
Chrnd TC 443-467 GID STN YIVKQIKEKNAYDEEVGNW
negative charge
positive charge
B
EC
IC
Vestibule
S435
D397
α3
β4
α5
C
β4
α3
α5
S435
D397
β4
α5
α3
D397

Figure 3

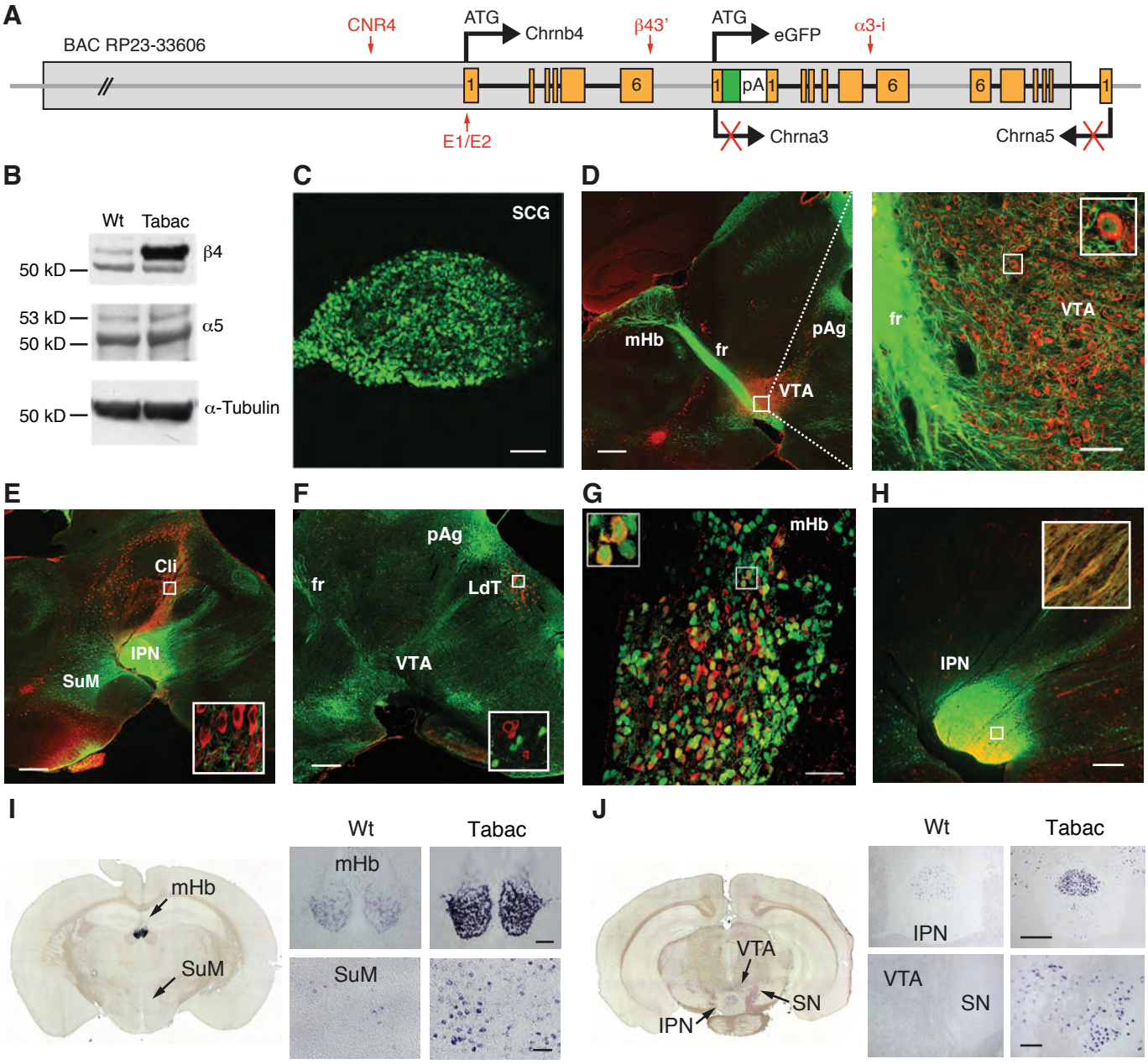
A
BAC RP23-33606
CNR4
ATG
Chrnb4
β43'
ATG
eGFP
α3-i
E1/E2
Chrna3
Chrna5
pA
B
Wt
Tabac
50 kD
β4
53 kD
50 kD
α5
50 kD
α-Tubulin
C
SCG
D
mHb
fr
pAg
VTA
fr
VTA
E
Cli
IPN
SuM
F
pAg
fr
LdT
VTA
G
mHb
H
IPN
I
mHb
SuM
Wt
Tabac
mHb
SuM
J
VTA
IPN
SN
Wt
Tabac
IPN
VTA
SN

Figure 4

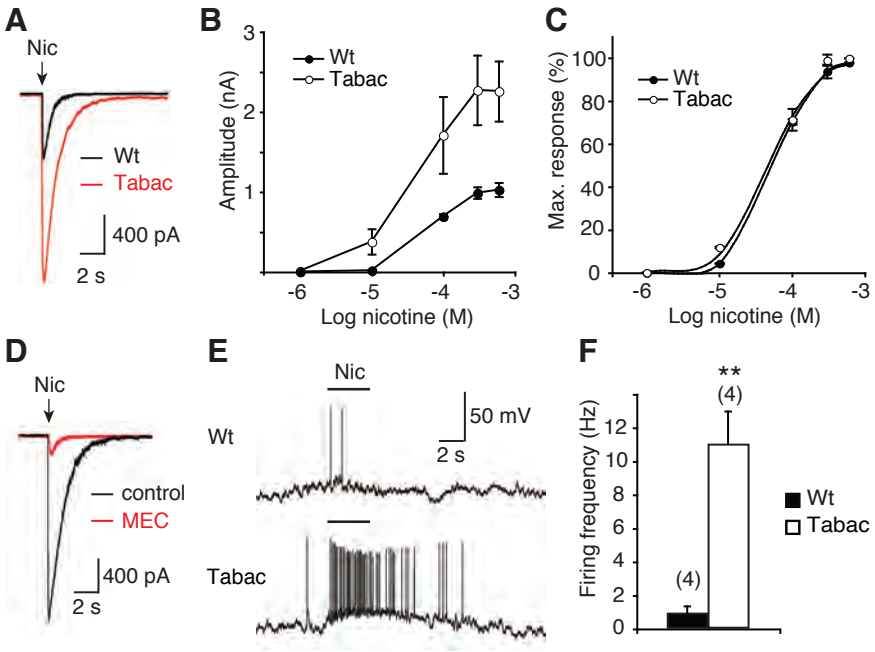
A
Nic
Wt
Tabac
400 pA
2 s
B
Amplitude (nA)
Wt
Tabac
Log nicotine (M)
C
Max. response (%)
Wt
Tabac
Log nicotine (M)
D
Nic
control
MEC
400 pA
2 s
E
Nic
Wt
50 mV
2 s
Tabac
F
**
(4)
(4)
Firing frequency (Hz)
Wt
Tabac

Figure 5

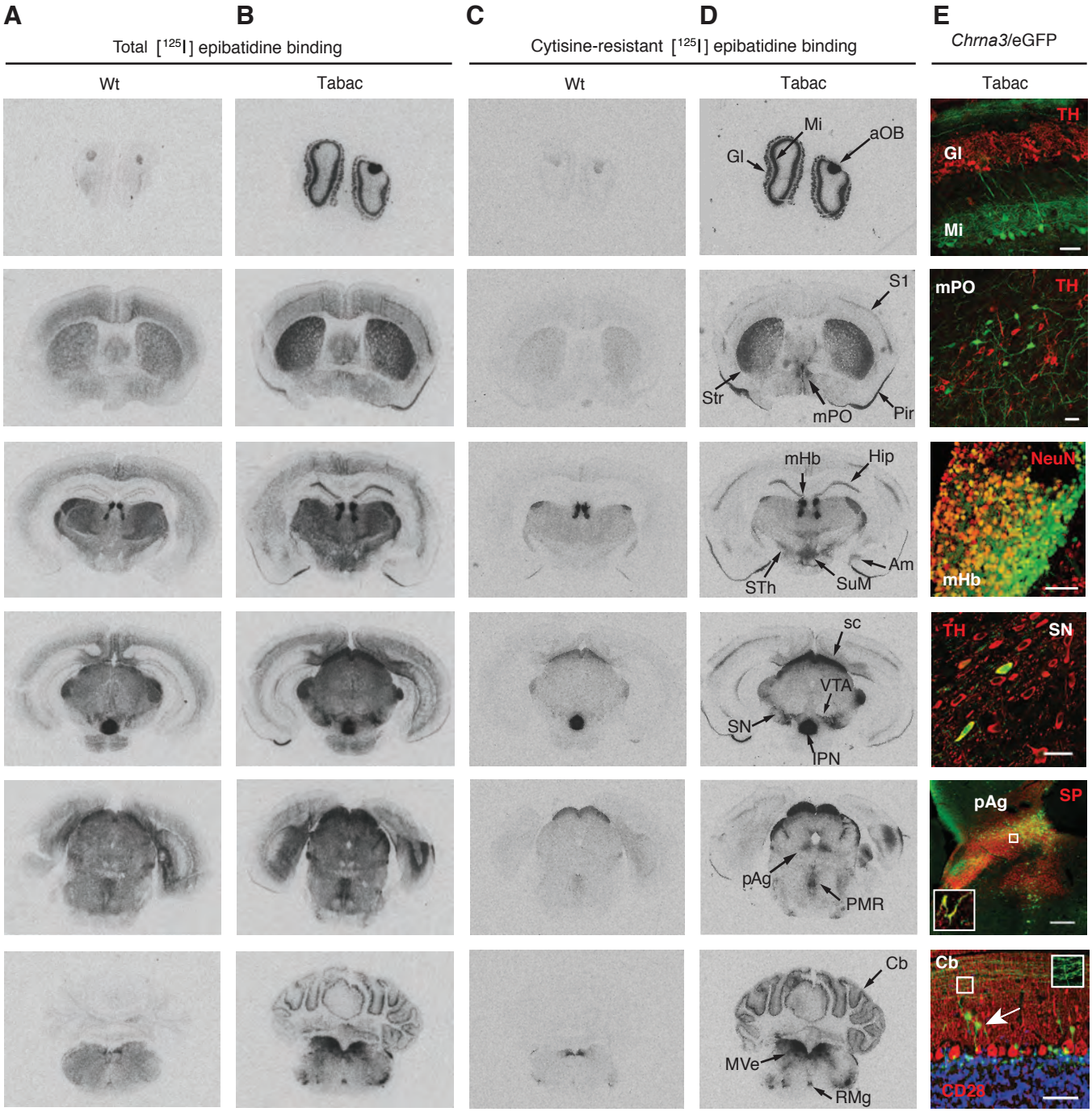
A
B
C
D
E
Total [125I] epibatidine binding
Cytisine-resistant [125I] epibatidine binding
Chrna3/eGFP
Wt
Tabac
Wt
Tabac
Tabac
Mi
aOB
Gl
TH
Gl
Mi
S1
Str
mPO
Pir
mPO
TH
mHb
Hip
STh
SuM
Am
NeuN
mHb
sc
VTA
SN
IPN
TH
SN
pAg
PMR
pAg
SP
Cb
MVe
RMg
Cb
CD28

Figure 6

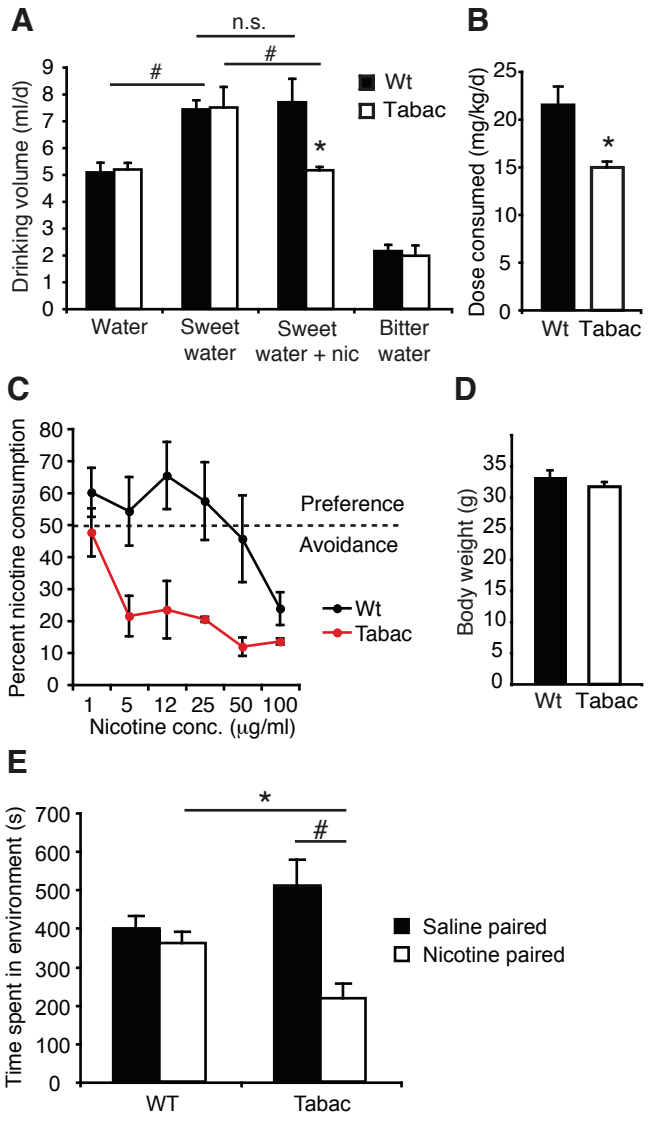
A
n.s.
#
#
Wt
Tabac
*
Drinking volume (ml/d)
0 1 2 3 4 5 6 7 8 9
Water
Sweet water
Sweet water + nic
Bitter water
B
Dose consumed (mg/kg/d)
0 5 10 15 20 25
*
Wt Tabac
C
Percent nicotine consumption
0 10 20 30 40 50 60 70 80
Preference
Avoidance
Wt
Tabac
1 5 12 25 50 100
Nicotine conc. (μg/ml)
D
Body weight (g)
0 5 10 15 20 25 30 35
Wt Tabac
E
*
#
Time spent in environment (s)
0 100 200 300 400 500 600 700
Saline paired
Nicotine paired
WT
Tabac

Figure 7

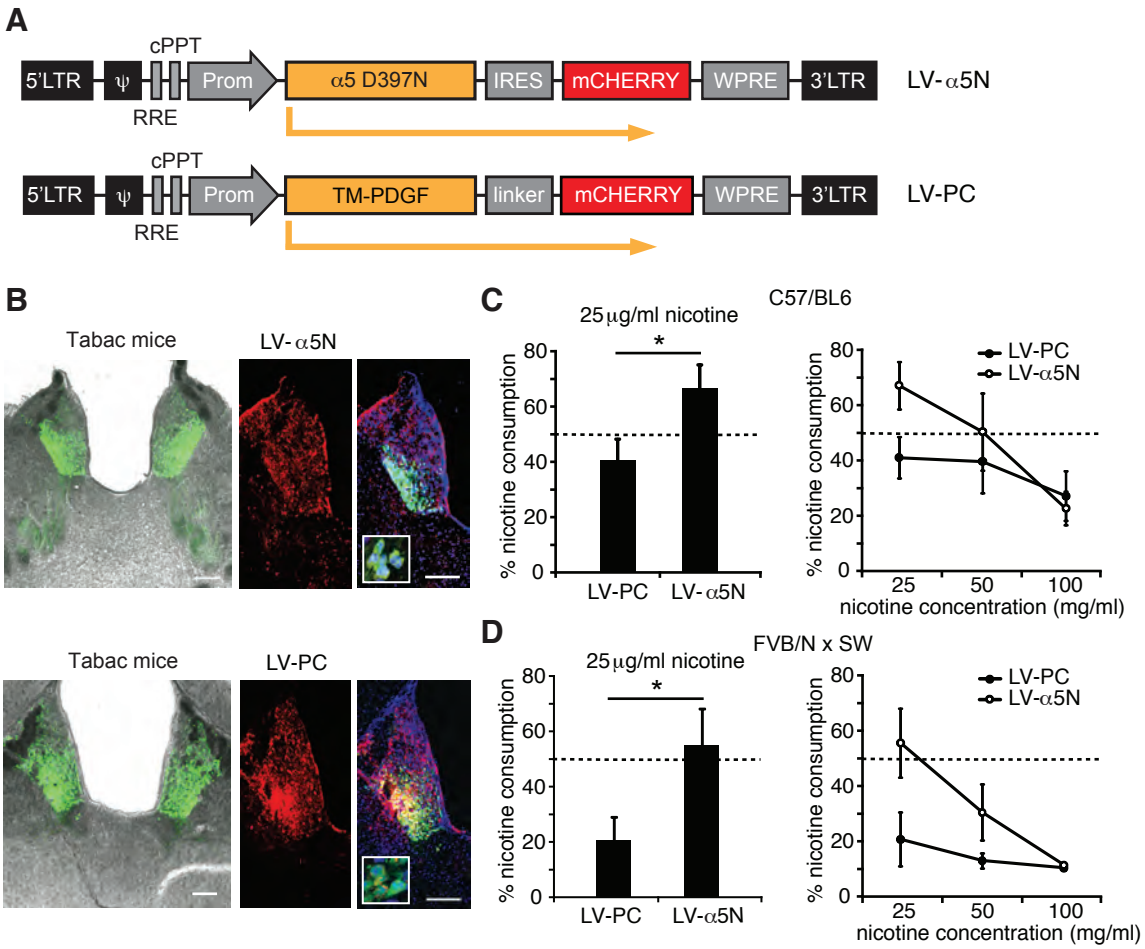
A
cPPT
5'LTR
ψ
Prom
α5 D397N
IRES
mCHERRY
WPRE
3'LTR
LV-α5N
RRE
cPPT
5'LTR
ψ
Prom
TM-PDGF
linker
mCHERRY
WPRE
3'LTR
LV-PC
RRE
B
Tabac mice
LV-α5N
Tabac mice
LV-PC
C
C57/BL6
25μg/ml nicotine
*
% nicotine consumption
LV-PC
LV-α5N
nicotine concentration (mg/ml)
D
FVB/N x SW
25μg/ml nicotine
*
% nicotine consumption
LV-PC
LV-α5N
nicotine concentration (mg/ml)

Supplemental Text and Figures

The supplemental data consists of 4 figures and 1 table.

Figure S1 is related to Figure 1

Figure S2 is related to Figure 3

Figure S3 and Table S1 are related to Figure 5

Figure S4 is related to Figure 6

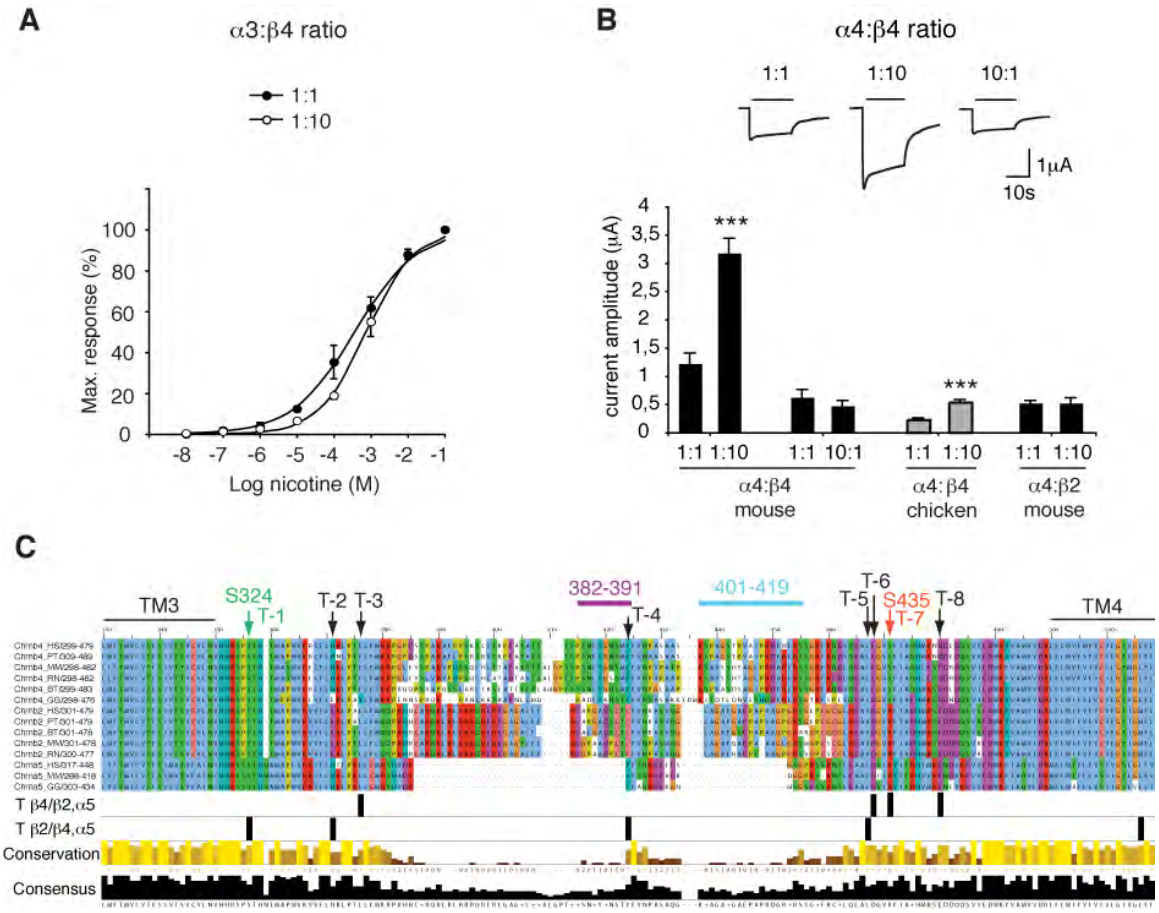

Figure S1. The rate-limiting effect of β4 is independent of the α-subunit and conserved between species

(A) Dose-response curves expressed as percent of maximal current amplitudes in response to nicotine in oocytes injected with 1:1 and 1:10 ratios of α3:β4.

(B) Representative traces of nicotine-evoked (bar: 100 μM nicotine for 20 s) currents recorded from Xenopus oocytes injected with mouse α4:β4 cRNAs at different ratios (upper panel). Ten-fold overexpression of mouse or chicken β4 relative to α4 significantly enhanced nicotinic responses compared to 1:1 ratios ($P < 0.001$). In contrast, overexpression of β2 (ratio 1:10) did not change nicotine-evoked currents in combination with α4. All values are expressed as mean ± s.e.m.; $n = 5$ per ratio in all experiments.

(C) Alignment of Chrnb4, Chrnb2 and Chrna5 protein sequences from different species reveals single differential aminoacids within highly conserved regions. A custom track T β4/β2,α5 shows the differential conservation scores of β4 sequences compared to β2 and α5 (the resulting differential residues were designated T-3 and T-6-8). T β2/β4,α5 shows the differential conservation scores of β2 sequences compared to β4 and α5 (the resulting differential residues were designated T-1-2 and T-4-5). The tracks below show the global conservation and the consensus residues. Two residues of β4 (S324 and S435,

green and red arrows) showing differential conservation score were selected for generation of β2-β4 chimeras shown in figure 5D. Abbreviations: Homo sapiens (HS), Pan troglodytes (PT), Mus musculus (MM), Rattus norvegicus (RN), Bos taurus (BT), Gallus gallus (GG), transmembrane domain (TM).

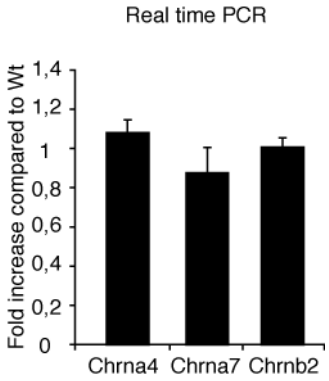

Figure S2. Normal transcriptional levels of *Chrna4*, *Chrna7* and *Chrnb2* in Tabac mice

Real time PCR using cDNA extracted from Tabac and Wt brains shows similar levels of transcription of Chrna4 (α4), Chrna7 (α7) and Chrnb2 (β2) in Wt and transgenic mice.

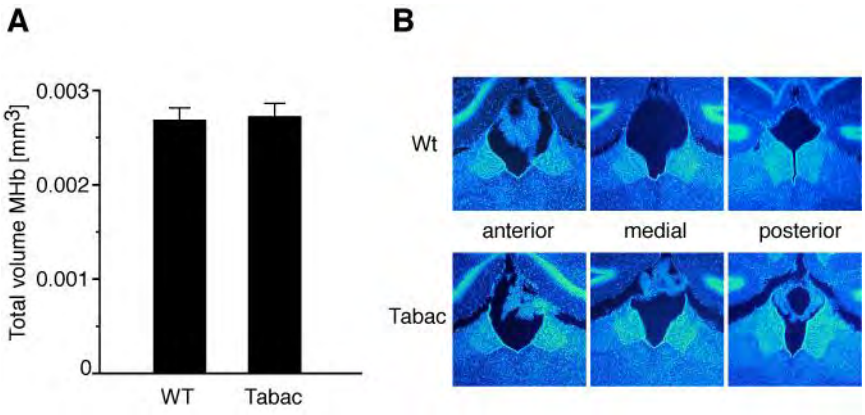

Figure S3. Cell number in the MHb of Tabac mice is unchanged

(A and B) Measurement of total MHb volume in Wt and Tabac mice (A), determined by area analysis of DAPI stained (B) serial coronal sections (21 sections per brain, 3 animals each).

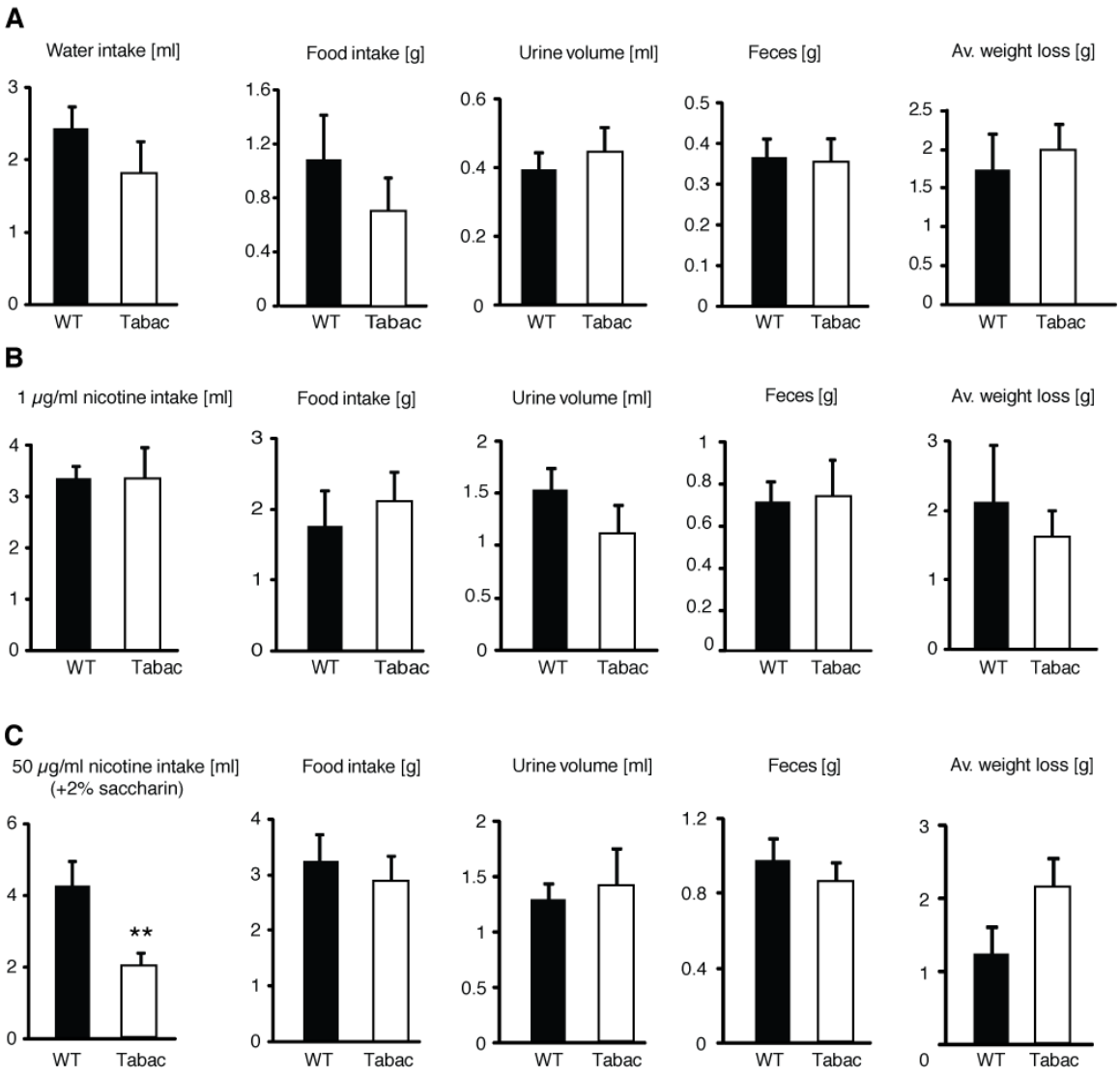

Figure S4. Digestion and micturition of Tabac mice are not altered

(A) No significant changes of metabolic rates were observed between Wt and Tabac mice when mice were given water. (B) Addition of a non-aversive dose of nicotine (1 μg/ml) in the drinking water does not alter liquid intake or urination between Wt and Tabac mice, (C) while an aversive dose of nicotine (50 μg/ml) significantly reduces liquid intake in Tabac mice ($P < 0.01$).

Table S1: Areas of increased* cytisine-resistant [^{125}I] epibatidine binding in Tabac brain

Brain region	**Optical density compared to Wt** (mean fold increase ± SEM)	**Fluorescent signal in Tabac brain**
Limbic system and related areas		
Amygdala (central, cortical and medial nuclei)	4,27 ± 1,40	cell bodies
Hippocampus (CA1)	4,21 ± 0,10	cell bodies
Piriform cortex	7,84 ± 1,07	cell bodies + processes
Entorhinal cortex	4,12 ± 0,69	cell bodies
Olfactory bulb (glomerular layer)	6,10 ± 0,73	processes
Olfactory bulb (mitral cell layer)	7,5 ± 0,59	cell bodies
Accessory olfactory bulb	2,37 ± 0,81	cell bodies
Dopaminergic system		
Striatum	4,77 ± 0,11	processes
Substantia nigra pars compacta	3,17 ± 0,37	cell bodies + processes
Ventral tegmental area	1,86 ± 0,05	cell bodies + processes
Cortex (S1, barrel cortex)	4,14 ± 0,51	cell bodies
Thalamus** and Hypothalamus		
Medial preoptic area	5,48 ± 1,00	cell bodies
Dorsomedial hypothalamic nucleus	3,89 ± 0,53	cell bodies
Supramammilary nucleus	4,66 ± 0,44	cell bodies
Subthalamic nucleus of the thalamus	3,51 ± 0,24	cell bodies
Midbrain**		
Periaqueductal gray (ventrolateral)	3,64 ± 0,55	cell bodies
Paramedian raphe nucleus	2,66 ± 0,55	cell bodies
Superior colliculus	1,48 ± 0,14	cell bodies + processes
Inferior colliculus	1,99 ± 0,17	cell bodies
Brainstem		
Vestibular nucleus	2,09 ± 0,04	cell bodies
Nucleus raphe magnus	5,24 ± 2,52	processes
Cerebellum		
Granule cell layer	9,51 ± 0,24	cell bodies and parallel fibers
Molecular cell layer	5,82 ± 1,68	cell bodies

* Student's t-test, $P < 0.05$, $n = 3$ per genotype

** Areas of saturated binding in Wt as medial habenula, lateral geniculate and Interpeduncular nucleus were not considered.

Supplementary experimental procedures

Differential conservation scores. Protein sequences were downloaded from the NCBI Protein database, aligned using clustalw (Thompson et al., 1994), and displayed with Jalview (Waterhouse et al., 2009). The sequence conservation C at each position in the alignment is defined as the difference between the maximum possible entropy and the entropy of the observed symbol distribution (Schneider et al., 1990). Considering two groups A and B of proteins, we define at each position in the alignment their respective conservation as C(A) and C(B), and their respective consensus residues as R(A) and R(B). The differential conservation score S = C(A) + C(B) if R(A) is not equal to R(B), S=0 otherwise. To focus on strong conservations, S was set to 0 if more than one mismatch was found in a group.

Real time PCR. Brains of littermates were dissected in ice-cold PBS and collected in Trizol. Total RNA was isolated and reverse transcribed using Moloney murine leukemia virus reverse transcriptase (Invitrogen) according to the manufacturer's instructions. Real-time RT-PCR was performed on the iCycler IQ^{TM} 5 multicolor real-time detection system (Bio-Rad), using absolute SYBR green fluorescein (ABgene). PCR program was carried out following the standard protocol. The primer sequences for each gene were designed as follows: β-actin 5'-TCG TGC GTG ACA TCA AAG AGA AGC-3' (forward), 5'- ATG GAT GCC ACA GGA TTC CAT ACC-3' (reverse); α4 5'-GCT CAG CTC ATT GAT GTG GA-3' (forward), 5'-GTC AAT CTT GGC CTT GTC GT-3' (reverse); α7 5'-TGC TCA TTC CTT GTG TGC TC-3' (forward), 5'-TGG TGA TAT CGC AGC ACA AT-3' (reverse); β2 5'-TGC TTT GTC AAT CCT GCA TC-3' (forward), 5'-TCA GTG GAG TGG GGA TCA AT-3' (reverse). Expression levels for the different genes were normalized to the expression level of β-actin and further normalized with respect to the levels in Wt. Duplicate samples were analyzed with the average values indicated as bars and positive value as error bars. All experiments were performed at least twice with similar results.

MHb volume measurement. 12 week old, male Wt and Tabac mice were transcardially perfused with 4% PFA and brains were incubated overnight in 30% sucrose. Floating cryosections with a

thickness of 50 μm were produced, and nuclei of cells were stained with DAPI for 1h. Sections were washed and mounted on glass slides. Fluorescent images were acquired with a Keyence Biozero BZ8100E and MHb area was determined by Image J. Finally, total MHb volume was calculated in Excel and corrected for overall brain weight before sectioning.

Metabolic rates. To assess the metabolic rate of adult (12 weeks) male FVB/N Tabac (*n* = 8) mice and their Wt (*n* = 8) littermates, mice were single housed in metabolic cages over night (Uno BV, Zevenaar, The Netherlands). Mice had *ad libitum* access to pelleted food and to a drinking bottle containing either water, 1 μg/ml or 50 μg/ml nicotine. Urine and fecal pellets were collected after 18h at the end of the active phase and their total weight was determined.

Supplementary references

Thompson, J.D., Higgins, D.G. and Gibson, T.J. CLUSTAL W: improving the sensitivity of progressive multiple sequence alignments through sequence weighting, position specific gap penalties and weight matrix choice. *Nucl. Acids Res*. 22: 4673-4680 (1994).

Waterhouse, A.M., Procter, J.B., Martin, D.M.A, Clamp, M. and Barton, G. J. Jalview Version 2 - a multiple sequence alignment editor and analysis workbench. *Bioinformatics* 25: 1189-1191 (2009).

Schneider, T.D. and Stephens, R.M. Sequence logos: A new way to display consensus sequences. *Nucleic Acids Res*. 18: 6097–6100 (1990).

ETOC Paragraph Neuron-D-11-0117:

Recently, heavy smoking and lung cancer has been associated to variations in the CHRNB4-A3-A5 gene cluster that encodes the $\alpha3\beta4\alpha5$ nicotinic receptor. In this study we show that mice overexpressing the $\beta4$ subunit have strong aversion to nicotine, which is reversed upon expressing the most common variant of $\alpha5$ associated to smoking, into the mibrain medial habenula of these mice. These studies are relevant to the human condition since they provide direct evidence that nicotine dependence can be controlled by these receptors.

Neuron Conflict of Interest Form

Cell Press, 600 Technology Square, 5th floor, Cambridge, MA 02139

Please complete this form electronically and upload the file with your final submission.

Neuron requires all authors to disclose any financial interest that might be construed to influence the results or interpretation of their manuscript.

As a guideline, any affiliation associated with a payment or financial benefit exceeding $10,000 p.a. or 5% ownership of a company or research funding by a company with related interests would constitute a financial interest that must be declared. This policy applies to all submitted research manuscripts and review material.

Examples of statement language include: AUTHOR is an employee and shareholder of COMPANY; AUTHOR is a founder of COMPANY and a member of its scientific advisory board. This work was supported in part by a grant from COMPANY.

Please disclose any such interest below on behalf of all authors of this manuscript.

Please check one of the following:

☒ None of the authors of this manuscript have a financial interest related to this work.

☐ Please print the following Disclosure Statement in the Acknowledgments section:

Please provide the following information:

☒ Please check this box to indicate that you have asked every author of this work to declare any conflicts of interest. Your answers on this form are on behalf of every author of this work.

Manuscript #: D-11-0117

Article Title: Aversion to nicotine is regulated by the balanced activity of β4 and α5 nicotinic receptor subunits in the medial habenula

Author List: Silke Frahm, Marta A. Slimak, Leiron Ferrarese, Julio Santos-Torres, Beatriz Antolin-Fontes, Sebastian Auer, Sergey Filkin, Stéphanie Pons, Jean-Fred Fontaine, Victor Tsetlin, Uwe Maskos, Inés Ibañez-Tallon

Your Name: Ines Ibanez-Tallon

Date: 6 April 2011